

FINAL
10-43-97
OCT
1997

Final Report to NASA

**Multi-Satellite Estimates of Land-Surface Properties for Determination of
Energy and Water Budgets**

NAGW-2973

under NRA 91-OSSA-07

October 1991-March 31 1997

Principal Investigator:

W. Paul Menzel

Co-Investigators:

Robert M Rabin (NOAA/NSSL/CIMSS)
Christopher M. U. Neale (Utah State University)
Kevin Gallo (NESDIS)
George R. Diak (SSEC/CIMSS)

Additional Contributors:

Barbara A. Burns (SSEC/CIMSS)
William Raymond (SSEC/CIMSS)
Chris Collimore (SSEC/CIMSS)
Changyi Sun (Utah State University)
Xin Qui (Utah State University)

Prepared by:

Robert M. Rabin
January 1998

Project Summary:

Using the WETNET database, existing methods for the estimation of surface wetness from SSM/I data have been assessed and further developed. A physical-statistical method for optimal estimation of daily surface heat flux and Bowen ratio on the mesoscale has been developed and tested. This method is based on observations of daytime planetary boundary layer (PBL) growth from operational rawinsonde and daytime land-surface temperature amplitude from Geostationary Operational Environmental (GOES) satellites. The mesoscale patterns of these heat fluxes have been compared with an AVHRR-based vegetation index and surface wetness (separately estimated from SSM/I and in situ observations). Cases of the 1988 Midwest drought and a surface/atmosphere moisture gradient (dry-line) in the southern Plains were studied. The analyses revealed significant variations in sensible heat flux (S_0 , and Bowen ratio, B_0) associated with vegetation cover and antecedent precipitation. Relationships for surface heat flux (and Bowen ratio) from antecedent precipitation and vegetation index have been developed and compared to other findings.

Results from this project are reported in the following reviewed literature.

- Diak, G.R., M.W. Whipple, 1994: A note on the use of rawinsonde data to estimate the daytime fluxes of sensible and latent heat: a comparison with surface flux measurements from the FIFE. *J. Ag. For. Meteor.*, 68: 63-75.
- Diak, G.R., M.W. Whipple, 1995: Note on estimating surface sensible heat fluxes using surface temperatures measured from a geostationary satellite during FIFE 1989. *J. Geophys. Res.*, 100, No. D12: 25453-25461.
- Diak, G.R., R.M. Rabin, K.P. Gallo, C.M. Neale, 1995: Regional-scale comparisons of vegetation and soil wetness with surface energy budget properties from satellite and in-situ observations. *Remote Sensing Reviews*, 12: 355-382.
- Segal, M., R.W. Arritt, C. Clark, R. Rabin, J. Brown, 1995: Scaling evaluation of the effect of surface characteristics on potential for deep convection over uniform terrain. *Mon. Wea. Rev.*, 123: 383-400.
- Burns, B.A., R.M. Rabin, G.R. Diak, W.H. Raymond, C.C. Collimore, C.M. Neale, 1997: Relating remotely-sensed vegetation and soil moisture indices to surface energy fluxes in the vicinity of an atmospheric dry-line. In preparation for submission to *J. Appl. Meteor.*

In addition, the following informal contributions have been published:

Neale, C.M.U., X. Qiu, C. Sun, K. P. Gallo, R. M. Rabin, and G. R. Diak, "Monitoring surface moisture and flooding in the central plains with the Special Sensor Microwave/Imager (SSM/I)," 2nd International Scientific Conference on the Global Energy and Water Cycle, Preprint Volume, 1996, pp. 217-218.

Neale, C.M.U., C. Sun, X. Qiu, G. Vassiliades, K. P. Gallo, and R. M. Rabin, "Surface moisture and temperature retrievals with the SSM/I: integrated physically and empirically-based approaches," paper presented in 5th Specialist Meeting on Microwave Radiometry and Remote Sensing of the Environment, Boston, MA, USA, 4-6 November 1996.

Neale, C.M.U., C. Sun, K. P. Gallo, and R. M. Rabin, "Long term soil moisture monitoring over the U. S. Using combined SSM/I and AVHRR datasets," paper presented in 5th Specialist Meeting on Microwave Radiometry and Remote Sensing of the Environment, Boston, MA, USA, 4-6 November 1996.

Sun, C. and C. M. U. Neale, "Mapping land surface type from SSM/I data with a dynamic database," paper presented in 5th Specialist Meeting on Microwave Radiometry and Remote Sensing of the Environment, Boston, MA, USA, 4-6 November 1996.

Xin Qiu, 1995: Synoptic Surface Moisture Retrieval Using Special Sensor Microwave/Imager (SSM/I) and Advanced Very High Resolution Radiometer (AVHRR) Data. PhD dissertation, Department: of Electrical and Computer Engineering, Utah State University, 181 pages.

1. Remote Measurements of Surface Wetness.

The initial method is based on regression between SSM/I brightness temperatures and an antecedent precipitation index (API), derived from the NOAA cooperative observer network of daily rainfall and temperature, and an empirical model for evapotranspiration. As reported by Neale et al. (1990), the ratio T_{19H}/T_{37V} using a maximum depth of soil moisture available for evaporation of 15 mm produced the highest correlation with the surface based API (.68). The algorithm is built on separate regressions for low, medium, and high vegetation density. For purposes of the API algorithm, the density is determined from the average polarization difference using 19 and 37 GHz brightness temperatures (Neale et al. 1990). The initial method was applied to the case studies reported in Section 3-4. Comparisons are made to spatial patterns of the surface energy budget inferred from satellite infrared measurements during clear-sky conditions. The initial algorithm has been enhanced to utilize a dynamic database in classifying the land-surface condition from a 3-day

running average polarization difference. The modified version is tested through direct comparison with the initial method and ground based API for the case study described in Section 4.

2. Surface Energy Budget Estimator

A procedure to estimate daytime surface sensible and latent heat fluxes from rawinsonde measurements of the time-change of the height of the planetary boundary layer interpreted by a surface layer-mixed layer model is outlined in Diak and Whipple (1994). The procedure was implemented using rawinsonde data at 12 and 00 UTC. Comparisons of derived fluxes with those measured from a network of surface stations during the First International Satellite Land-Surface Climatology Project (ISLSCP) Field Experiment (FIFE) indicated standard errors of estimation of 1.2 and 1.5 MJm⁻², respectively, for the 12-hr sensible heating and evapotranspiration totals. (A typical combined sensible and latent heating total for a clear summer day in mid-latitudes is about 15 MJm⁻²). The procedure captured a 2-3 fold increase in sensible heat flux associated with rapid drying of the surface during a 7-day period following rainfall.

The use of surface heating rates from satellite measured skin temperatures to infer surface sensible heat flux has been demonstrated by Diak and Whipple (1995). Matching observations of daytime surface temperature range from the geostationary GOES with output from a surface and PBL model, estimates of daytime sensible heat flux were made for fixed values of roughness length. Comparisons made with the same FIFE surface data indicated similar magnitude in standard errors of estimate as with the approach of using rawinsonde measurements of the time-change of planetary boundary layer height. The standard errors in 12-hr (daytime) sensible heating estimates are within about 1.5 MJm⁻² of the FIFE surface-based measurements for the days which we investigated for the mixed prairie environment. This level of information is somewhat better than projected in a prior study (Diak and Stuart 1989). There are also some indications from measurements made at the FIFE site of remotely-sensed temperatures with time and viewing angle, that the use of temporal changes may also reduce problems associated with angle of view (see Fig. 3a, Diak et al. 1995).

A prototype "statistical estimation" procedure was implemented to estimate surface sensible and latent heating values (Diak et al. 1995). An extension of methods described in Diak (1990) and Diak and Whipple (1993), the procedure uses both the measurements of surface heating rates and boundary layer growth described above as an information base and models of the surface

and atmosphere as vehicles to interpret these measurements. It is applied to the estimation of either the 12-h surface Bowen ratio (B_0 , the ratio of sensible to latent heat) or the surface sensible heat flux (S_0) itself and the effective surface roughness length (Z_0) from the two measurements, the temporal change in surface skin temperature (DT_s) and the temporal change in boundary layer height (DH). The scheme utilizes a “forward” surface/PBL model which predicts DT_s and DH as a function of prescribed surface S_0 (or B_0) and Z_0 . In matrix form, the optimal estimation algorithm can be written:

$$x = x_b + C * K^T * (K * C * K^T + E)^{-1} * (y_m - y_{xb}), \quad (1)$$

where the superscript T indicates a matrix transpose and superscript -1 a matrix inverse, and:

x = a column vector, the elements of which are the quantities to be estimated (B_0 , Z_0)

x_b = a column vector with "background" or prior information values of B_0 and Z_0 from climatology or other sources. In this study, they were set to unity and 5 cm respectively.

y_m = a column vector of measurement quantities (DT_s , DH).

y_{xb} = a column vector of estimates of measurement quantities (DT_s , DH) made from the background values of B_0 and Z_0 using the forward model.

C = a matrix of error covariances of the background quantities of B_0 and Z_0 contained in x_b . The corresponding error variances were set to represent the entire physical range of the two quantities. Hence, for this study, the estimation procedure is unconstrained by the background variables, hence, the off-diagonal terms in the C matrix are zero.

K = a matrix of derivatives of the measurement quantities (DT_s , DH) with respect to the estimated quantities (B_0 , Z_0) from the forward model (e.g., $d(DT_s)/d(B_0)$, etc.). These derivatives indicate how the retrieval values B_0 and Z_0 should be adjusted given a change in the measured variables DH and DT_s from the prior estimates ($y_m - y_{xb}$). For example, in the always positive (a higher value of the Bowen ratio and sensible heating produce higher values of the PBL height), indicating that a positive value of ($y_m - y_{xb}$, e.g., measured greater than prior estimate) should result in a positive adjustment to the Bowen ratio (more sensible heating in the retrieval process).

E = a matrix of errors in measurement quantities (DT_s , DH) that are the sum of measurement errors plus errors in the forward model that produce estimates of the measurement variables (DT_s , DH) from the retrieval quantities (B_0 , Z_0). The error variance of DH is set to 200m based on published studies by Driedonks (1982 a,b). For DT_s , the error variance is prescribed to vary linearly from 2 C at a measured DT_s of 5 C, to 4 C at a measured DT_s of 20 C. This is based on empirical information that higher

surface temperature time changes occur for dry and aerodynamically smooth surfaces, where prediction model accuracy suffers.

Other important features of this statistical estimation technique are as follows:

- Estimates of surface quantities were performed on a regular grid (the grid of the CIMSS Subsynoptic Scale Forecast Model, SSM), with a horizontal resolution of about 80 km for the Midwest drought case, 40 km for the Southern Plains case.
- DH data is produced by procedures which evaluate the height of the PBL at rawinsonde locations at 12 UTC and following 00 UTC times and differing the two values.
- A 1-d PBL model (Diak and Whipple, 1993) is also used at rawinsonde locations to establish the other required parameters which adjust for local meteorological conditions and make estimates of the measurement quantities from the surface quantities to be estimated (the K matrix)
- The DH measurements made at the rawinsonde locations and the model-predicted quantities (elements of the K matrix and model-predicted values of DH and DT, for various B_0 , Z_0 combinations) are analyzed to the SSM grid.
- DT, data and a clear/cloudy mask are diagnosed by automated procedures from GOES data. DTs is evaluated as the maximum daytime skin temperature minus the temperature evaluated three hours after local sunrise at each model grid location. The DT, data are at a high horizontal resolution compared to the grid (~4km). The DT, data are averaged around the model grid point locations to make suitable 80 km (40 km) averages. Surface S_0 , B_0 and Z_0 estimates are only performed at clear locations (e.g., where there is both DT, and DH information).

3. Midwest Drought Case

The surface energy estimator was applied a large region of the central U.S. on an exceptionally clear day (6 June, 1988) during the midwest drought of 1988 (Diak et al. 1995). The region is bounded roughly between 35-45 N and 75-105 W.

a. Relation of DT, to NDVI and API

We evaluated the Normalized Difference Vegetation Index (NDVI) at 1 km resolution from AVHRR data from NOAA-10 (Local Area Coverage, LAC) available on the previous day, 5 June 1988, which was also quite clear. The NDVI was computed using the pre-launch sensor calibrations.

No corrections were made for atmospheric effects such as humidity or aerosols. For statistical comparisons with other surface quantities, the NDVI data was analyzed to a uniform latitude-longitude grid of 0.25 degrees. Many research studies have examined measurements of vegetation index along with collocated measurements of absolute skin temperature (T_s) over much smaller domains. To our knowledge, this was the first study to examine *time changes* of the skin temperature, DT_s , along with the vegetation index.

The most obvious relationship between NDVI and DT_s is over the eastern two thirds of the region (Fig 4b, Diak et al. 1995), where the contour lines of DT_s follow quite closely the gradations of NDVI, with low (high) values of DT_s associated with high (low) values of NDVI. Even at the relatively coarse scale of the spatially-averaged GOES data, smaller local increases in NDVI, such as that on the Iowa-Missouri border, show up as local depressions in the daytime temperature range. The highest values of surface temperature range in this region are associated with the lowest NDVI regions in Illinois, Indiana, and the Minnesota-Iowa border, presumably containing the least vegetation and most bare soil exposure. These areas were also found to have the highest amount of Outgoing Longwave Radiation (OLR) during the month of June 1988 from wideband IR measurements from ERBE satellites and estimated from GOES narrowband estimates. In contrast, the northwestern corner of the domain has generally low NDVI values but also low values of DT_s , the opposite of the relationship observed in the eastern region for areas with low NDVI.

For the entire domain, the correlation between NDVI and DT_s is poor (correlation coefficient=-0.38). As discussed, however, the relationship between NDVI and DT_s in the east appears stronger, and for that region (east of 95 degrees longitude) the correlation coefficient between the two was found to be -0.84. West of this longitude, much of the western area has regions with low values of NDVI and the correlation between NDVI and DT_s is poor (correlation coefficient= -.35). The difference in character of the NDVI versus DT_s between the eastern and western regions appears to be caused by the differing behavior of the surfaces with the most bare soil exposure (low NDVI values).

Investigation of the difference in the character of the surface based API values (API_s) between the eastern and western regions helps to explain the differing temperature response in the low NDVI range. In the east, the API_s values are generally very low in this drought of

1988, indicating that the surface layer soil moisture is limited, while in the west the average API, values are higher. Over the whole domain, the correlation of DTs with APIs is low (-.35). For locations with the lowest NDVI values (in the range of $NDVI < .25$), however, the correlation between DTs and API, improves significantly (correlation coefficient=-.74).

The shape of the scatter plot of DT, versus NDVI shown in Fig. 5 of Diak et al. (1995) can be explained in the following manner. For high NDVI values, which represent land surfaces with dense vegetation, the daytime surface temperature range, DT_s, is a minimum. For these vegetated surfaces, the temperature range is reduced both by the generally significant fraction of the net radiation partitioned into evapotranspiration and also by their aerodynamically rough character, which increases the transfer efficiency of turbulent exchange with the atmosphere. This combination of processes acts to reduce the surface skin temperature range and keep its variability low for vegetated surfaces.

The variability of the surface temperature range in the low NDVI regime is at a maximum, due to the variations of the sensible/latent heat balance as conditions vary from very wet to very dry in these bare soil land surfaces. The aerodynamically smooth character of bare soil surfaces compared to vegetation also means a low turbulent transfer efficiency with the atmosphere and a comparatively large daytime temperature range for an equivalent sensible heating total, compared with a vegetated rough surface. Overall, the variability in DT_s is poorly explained by NDVI variations within this low NDVI range, however, values of DT_s and API_s show a higher correlation.

Other factors can also contribute to scatter in the plot of DT_s versus NDVI. Different regions with similar NDVI values can have vegetation of different types and distributions, and thus different surface radiometric temperature response for identical surface energy balance conditions. Also, the DT_s observations have not been normalized for variations in the meteorological conditions (including wind speed and horizontal advection of temperature) or net radiation over the large area investigated in this study.

Despite these caveats and that both the NDVI and DT_s information have been averaged to a relatively coarse resolution, the general shape of the relationship is quite similar to that shown at between higher resolution (1 km) collocated measurements of absolute skin temperature and NDVI (Carlson et al. 1993; Nemani et al. 1993; Gillies et al. 1997), made over smaller horizontal areas. Compared to these studies, our DT_s versus NDVI relationship exhibits more scatter. This is to be

expected, since a greater range of soil and vegetation regimes, soil and moisture states and meteorological conditions are included than in the previous studies. Carlson et al. (1993) and others have used $T_s/NDVI$ relationships to estimate the surface energy balance. The larger variations in conditions here would need to be accounted for in applying similar techniques to this more extensive domain. The stronger correlation of DT_s with API_s in the low NDVI range suggests that some combination of NDVI and API_s might be used for a better description of the surface temperature and the energy balance than is achievable using the NDVI measurements alone. This is investigated in later sections.

b. Microwave-Based API Comparisons

The microwave-based API (API_m) was evaluated from SSM/I data at 1800 LST 6 June 1988 following the initial technique presented in Section 1. These estimates are more uniformly distributed than API_s within the region covered by the SSM/I overpass. The microwave has the potential to provide additional data where the surface-based measurements are sparse (e.g., the western Dakotas, Minnesota) and may also sense the effects of irrigation, whereas this would not be represented in API_s . Limiting the analysis to areas with relatively low NDVI ($< .25$), the comparisons of API_m with DT_s appear to be similar to those between API_s and DT_s . For comparisons east of 95 degrees longitude, the correlation is quite high (-0.85) and this correlation is slightly higher than that between DT_s and API_s for the eastern region and low NDVI range. This improved relationship with DT_s gives credibility to the microwave measurements and their potential in remote sensing surface energy budgets in agricultural regions when vegetation cover is low. West of 95 degrees longitude, the relationship between API_m and DT_s is less pronounced. The observed values of DT_s are a few degrees lower than over the eastern region for a similar range of API_m (0-5 mm). The change of DT_s with API_m is also much smaller there. The reason for the different behavior in the western area is as yet unclear. Previous studies have indicated the potential of deducing information on the soil wetness and evapotranspiration fraction (of available energy) from individual microwave brightness temperatures (T_b) at longer wavelengths than available with the SSM/I. The results of Kustas et al. (1993b) suggest that the relationship between T_b (21-cm wavelength) and evapotranspiration fraction is site-dependent and is limited by vegetation cover and subsurface soil moisture for the semiarid rangeland which they investigated. The measurement of subsurface soil moisture is a more acute

problem with SSM/I data. These limitations could be a factor in explaining the anomalous relationship between DT_s and API_m in the western region under investigation. Site-dependency may account for similar behavior between DT_s and API_s . Further more detailed investigation is required to explain the results over the western area.

c. Surface Energy Balance and "Effective" Roughness from DH and DT_s

The 12-hour average Bowen ratio (B_0) estimated from the method described in Section 2 in general follow the characteristics of the DT_s and DH data from which the Bowen ratio estimate is made (Figs. 4 and 8, Diak et al. 1995). A pronounced minimum of B_0 is evident in eastern South Dakota (where both DT_s and DH data showed their lowest values and also where API_s values were relatively high). Moving away from this minimum in both the northwesterly and northeasterly directions, both DT_s and DH show larger values, as do the corresponding B_0 estimates. Southeast of the minimum, moving through the region of the Minnesota-Iowa border through central Illinois, generally higher values of the measurement quantities of DH and DT_s also result in higher Bowen ratio estimates for the regions. At this time, the drought conditions which persisted through most of the Summer of 1988 in the Midwest were beginning to develop. DH estimates level off in this region at values of about 1400-1700 m and variations in the surface Bowen ratio estimates on the order of 0.1-0.2 coincide with smaller local maxima and minima in DT_s , such as the min/max couplets in the region of the northern Missouri border and the smaller temperature maxima along the northern Kentucky border.

While a qualitative comparison of the estimated B_0 values to the measurements (DT_s , DH) which enter into the estimation procedure are encouraging and a general agreement with the known developing drought conditions in the Midwest is evident in the derived B_0 field, quantitative comparisons with the other data sources are less conclusive. Over the whole domain, the correlation of B_0 values with collocated NDVI values is only -.30 and partitioning the comparison using various ranges of NDVI or latitude/longitude (as was informative in the previous comparisons of NDVI with DT_s) does not improve this result significantly. Certain "questionable" regions are evident in the B_0 field, such as in east-central Kentucky, where the highest estimates of B_0 on the domain have been produced, but where there is also considerable vegetation, as evidenced in the higher NDVI values.

The high values of B_0 here are the result of the high analyzed values of DH (Fig. 4c), which are mostly influenced by measurements made at two synoptic stations in the region, station 72433 in south central Illinois (DH=1695m) and station 72327 close to the Tennessee-Kentucky border (DH=1717m). The consistency of these two high DH measurements gives some creditability to the estimated B_0 values in the region and it is possible under conditions of developing drought to have a disparity between a vegetation index such as NDVI and the expected low values of the Bowen ratio (higher values of evapotranspiration). The region in question is in fact mostly devoted to agricultural crops, which might evidence higher Bowen ratio values when near-surface soil moisture becomes limiting, especially at this time near the beginning of the growing season when the rooting zone of the crops is still relatively shallow.

It is also possible in these first stages of development of the estimation methodology for B_0 and the effective roughness, Z_0 , that there are inconsistencies in the use of the two data sources DT, and DH which may contribute to the existence of "questionable" regions such as the example region discussed above. DT, data, even averaged to the 80 km we have used here, are still of a very high spatial scale when compared with the DH data, evaluated at radiosonde locations which have approximately a 400 km spacing in the continental United States. While the value of DH at a radiosonde location over a 12-hour period responds to an areal-average surface energy balance for a larger region than just the point location of the radiosonde observation (Norman et al. 1993), exactly how the information from these measurements should be spread out in space is as yet poorly understood. In this first effort, we have analyzed the DH values from the radiosonde measurements onto a uniform grid and in the B_0/Z_0 estimation procedure have not included data density weights reflecting the distance from grid points to the actual DH observation (radiosonde) locations. Thus for example, it may be possible that the DH measurements from radiosonde stations 72433 and 72347 discussed above, which are both close to high NDVI gradient areas in Kentucky, are being generalized to an overly large region. This may result in overestimates of the Bowen ratio in the region where high NDVI values suggest that lower B_0 values would exist.

Values of the effective surface roughness (Z_0 , mm) derived by the estimation procedures are shown on Fig. 8b in Diak et al. (1995). Regarding roughness estimates and the two information sources DT, and DH, much of the information on roughness under most observing conditions comes from the measurements of DT, as interpreted by the planetary boundary layer model which is used in

the estimation procedures (a sensitivity analysis of our B_0 and Z_0 estimation procedures has been presented in Diak and Whipple, 1993b). DH measurements also contain some information on the surface roughness, which are the result of changes in the PBL height brought about by mechanical turbulence effect (momentum exchange at the surface), but these influences are usually secondary. The correlation of values of Z_0 obtained in these procedures to the surface temperature range, DT_s , is -0.41. The correlation of Z_0 and NDVI over the entire domain, however, is 0.74 and it is interesting that this correlation coefficient is higher than both the mentioned Z_0/DT_s correlation (-0.41) and the NDVI/ DT_s correlation (-0.38, discussed in the previous section). Some prior evidence for such a relationship between spectral vegetation indices and the aerodynamic roughness has been presented by Moran (1990). It is the goal of this estimation system to partition the "signals" of DT_s and DH into estimates in the derived surface quantities, the Bowen ratio and effective roughness, using a surface/boundary layer model to account for local meteorology and other local dependencies. The general dependence of the surface roughness on vegetation cover and the correlation of the roughness derived from the estimation system to NDVI found in these results suggests that the prototype system is performing this function.

While the horizontal gradients of Z_0 appear consistent with vegetation patterns, the absolute roughness length results, however, do appear to have a low bias when compared with expected results from published studies for various vegetation classes (see, for example Oke, 1978). There is a large swath through central Iowa into Illinois where Z_0 is evaluated at 5 mm or less and the maximum values on the domain are only about 100 mm. At this point in time, the planetary boundary layer model which establishes the dependencies of the measurement quantities (DH , DT_s) on the surface energy budget, roughness and local solar forcing and atmospheric conditions does not include separate roughness lengths for heat (Z_{0h}) and momentum (Z_{0m}). Including a dependency of the sort $Z_{0m} > Z_{0h}$, as many studies have suggested is appropriate for natural surfaces (see, for example Garratt and Hicks 1973), would have the desired effect of raising the estimated values of the effective surface roughness.

4. Southern Plains Dry-Line Case.

The surface energy budget estimator was also applied to a region of the southern U.S. Plains on two consecutive days (26-27 May) in 1991. This case was chosen because of the west to east

gradient in surface vegetation and the accompanying atmospheric moisture distribution across the region. An atmospheric 'dry-line' was present on both days and together with meso-scale features in the land use is believed to have played a role in the initiation of localized convective storms along the western Oklahoma border on 26 May (Hane, et al. 1997). The domain chosen for this analysis is from 30-40 N and 90-110 W. The data characteristics are identical to those utilized for the Midwest case (Section 3), except that the geostationary satellite infrared data is from GOES-8 and the NDVI is the maximum values during a 2-week period in late May 1991 available from the USGS/EROS data center in Sioux Falls, S.D. The resolution of the analysis was increased to 40 km for this case. Comparison of preliminary results at 80-km and 40-km grid spacing showed that the 40-km grid provided better definition of spatial patterns, especially near cloudy areas with no apparent increase in noise. This implies that the infrared data provide sufficient spatial information to support analysis at this resolution.

a. Relationships Between Observed Variables.

The DT_s observations are compared to NDVI and API values at each clear-sky grid point. For the entire domain, the correlation of DT_s with NDVI is -.89 and -.83 and of DT_s with API is -.68 and -.67 for the two days, respectively. The most significant correlation between DT_s and API (-.65 and -.51) is where NDVI is less than .36, while the correlation is only -.28 and -.07 for NDVI greater than .36. These results are qualitatively similar to the those of Diak et al. (1995), while the satellite temperature signal is even more correlated with variations in soil moisture.

On both days, DT_s appears to be highly correlated with NDVI and API to the west of 97 W. To the east of this longitude, the correlations are quite small. Wetzel et al.(1984) have observed a similar geographic dependence of the correlation of skin temperature with API in Kansas. The climate to the east of 97 W is relatively humid and is characterized by high values of NDVI with less spatial variability as compared west of 97 W. The low correlation of DT_s to NDVI in the east is likely a result of the small range of NDVI in this area. Also, the level of NDVI is too high for API to be a factor on DT_s, hence the low correlations between DT_s and API. To the west, the climate is relatively dry and a strong gradient of NDVI exists.

b. Energy Variables.

The optimal estimation procedure was applied to the DH and satellite DT_s measurements to obtain estimates of S₀, B₀, and Z₀. In principle, this method could also be used to obtain estimates of the latent heat flux (LH), and the Bowen ratio could then be derived from the ratio S₀/LH. However, because the PBL model is forced primarily by the sensible heat flux such that the latent heat flux is derived as a residual in the surface energy budget given modeled values for the net radiation in clear sky areas and ground heat flux, the estimator is not very sensitive to LH. More accurate estimates of Bowen ratio are therefore derived directly with the optimal estimation method.

From examination of simple correlations, B₀ and Z₀ are both strongly correlated with DT_s, with correlation coefficients above 0.8 on 26 May 1991. On the following day, the correlation of B₀ with DT_s is also large for B₀ less than 4.0. Very high values of B₀ (> 4.0) were located in the northwest corner of the region. The correlation of Z₀ with DT_s is smaller on this day (.50). In addition, the values of Z₀ are generally higher on the 27 May than on the previous day. Although the cause of these differences in Z₀ are not known, it is possible that missing wind observations from a rawinsonde location in central Oklahoma on 27 May could have played a role.

The resulting spatial maps of S₀, B₀ and Z₀ (Fig. 1) show patterns expected from land cover variations in the area: high B₀ and S₀ in grassland areas; low B₀ and S₀ in agricultural areas. Also, the boundary between low and high B₀ (~1.5) corresponds with the location of abrupt airflow change observed in aircraft measurements on the previous day (Figs. 9-10, Hane et al. 1997). This supports the interpretation from their paper that developing convection and spatial perturbations in moisture, temperature, and wind observed on that day are associated with differences in land use and sensible heat flux (and Bowen ratio) in vicinity of the dry-line.

c. Relationships of B₀ and Z₀ to Vegetation and Moisture Indices

Figures 2-5 present scatter plots of estimated B₀ and Z₀ versus NDVI and API. The distribution of B₀ with respect to NDVI and API indicates that B₀ is most sensitive to changes in NDVI for lower moisture and lower canopy conditions: for NDVI > .4 and API > 20, B₀ changes very little. As expected, the relationship between Z₀ and NDVI is approximately linear and shows almost no dependence on API. The correlation of Z₀ with NDVI is about .80 on 26 May, but only .50 on 27 May. This much smaller correlation on 27 May is again related to unusually high values of

Z_0 computed on that day in areas with intermediate values of NDVI. Some of this area is not included in the 26 May analysis because of cloud cover.

To quantify the dependence of B_0 and Z_0 on both API and NDVI, a multilinear regression analysis was carried out from data on 26 May only. In the case of B_0 , three fits are given by the following equations:

for all API & NDVI:

$$\log(B_0) = 3.04 - 2.10 \log(\text{NDVI} \cdot 100) - 0.126 \log(\text{API}) \quad (2)$$

for all API, $\text{NDVI} < 4$:

$$B_0 = 3.50 - 7.03 \text{NDVI} - .42 \log(\text{API}) \quad (3)$$

for $\text{API} < 5$, $\text{NDVI} < 4$:

$$B_0 = .389 \cdot (40 - \text{NDVI} \cdot 100)^{.562} \quad (4)$$

For Z_0 , the following produce similar fits to the data:

linear:

$$Z_0 = -2.33 + 27.80 \text{NDVI} + .449 \log(\text{API}) \quad (5)$$

log:

$$Z_0 = -24.54 + 21.18 \log(\text{NDVI} \cdot 100) + 0.300 \log(\text{API}) \quad (6)$$

These relationships are plotted on scatter diagrams of B_0 and Z_0 vs. NDVI in Figures 2 and 4 for May 26 and 27, respectively. The fits from 26 May provide a reasonable representation to the scatter of data on May 27, indicating some day-to-day robustness of the relationships. These figures also illustrate how heat flux variables (in this case B_0) can be derived from NDVI given moisture information.

d. Relationships for Sensible Heat Flux.

Similar regression analyses, using the complete range of API and NDVI values, have been performed between sensible heat flux (S_0) and DT_s , NDVI, API. The polynomial coefficients,

correlation coefficients, and rms errors are given in Tables 1-3. The polynomials are shown on scatter plots in Fig. 6.

As seen from the scatter plots, S_0 is highly correlated with DT_s (correlation coefficient > 0.93). A higher order polynomial (Eq. 7) used in the fit is required to represent the asymptotic behavior seen in the scatter diagram.

$$S_0 = a_0 + a_1 * DT_s + a_2 * DT_s^2 + a_3 * DT_s^3 \quad (7)$$

Apparently, the influence of DH on the point-to-point variability of S_0 is too small to significantly lower the correlation of S_0 with DT_s . Despite this high correlation, there is a large variation in a_0 between the 2 days, suggesting a dependence on daily mean temperature. This supports the need for the surface/PBL model to determine S_0 from DT_s and other meteorological observations.

TABLE 1. Regression statistics: S_0 versus DT_s .

Date	a_0	a_1	a_2	a_3	r	rms
26 May	-1.39	.53	.017	-.00091	.983	.230
27 May	-.055	.126	.058	-.00196	.970	.459

Second order polynomials are used to model the relationships between S_0 and NDVI and between S_0 and $\log(\text{API})$,

$$S_0 = a_0 + a_1 * \text{NDVI} + a_2 * \text{NDVI}^2 \quad (8)$$

$$S_0 = a_0 + a_1 * \log(\text{API}) + a_2 * \log(\text{API})^2 \quad (9)$$

TABLE 2. Regression statistics: S_0 versus NDVI.

Date	a_0	a_1	a_2	r	rms
26 May	13.3	-27.7	12.3	.888	1.44
27 May	14.8	-31.2	14.2	.854	2.11

TABLE 3. Regression statistics: S_0 versus $\log(\text{API})$.

Date	a_0	a_1	a_2	r	rms
26 May	7.53	-1.81	-.958	.67	3.75
27 May	7.38	-2.73	-.599	.62	4.80

The correlation of S_0 with NDVI is in general higher than that with API (.8 vs. .6). The rms is about twice as high in applying the API regression (4 MJm^{-2}) than with the NDVI one. These results are qualitatively similar to that found in relating B_0 with NDVI and API in the Midwest drought case.

The regression was repeated with a cubic term, $a_3 \cdot \text{NDVI}^3$, added to (8). Only a modest improvement in the fit is observed. As with the analysis of Bowen ratio, we attempt to account for the combined effects of NDVI and API with a multivariate regression of S_0 against both NDVI and API. The results for the second order polynomial model (Eq. 10) are given in Table 4.

$$S_0 = a_0 + a_1 \cdot \text{NDVI} + a_2 \cdot \text{NDVI}^2 + a_3 \cdot \log(\text{API}) + a_4 \cdot \log(\text{API})^2 \quad (10)$$

TABLE 4. Regression statistics: S_0 versus NDVI and API.

Date	a_0	a_1	a_2	a_3	a_4	r	rms
26 May	12.7	-21.9	7.94	-.451	-.352	.901	1.28
27 May	13.9	-25.3	9.80	-.756	-.284	.868	1.92

The regression was repeated with a cubic term, $a_5 \cdot \text{NDVI}^3$, added to (10). Only a modest improvement in the fit is observed. Overall, the correlation is slightly higher (.9) and the rms slightly lower (1-2) than in separate regressions with NDVI and API. The best fit polynomials and associated data are shown in Figs. 7 and 8. In Fig. 7, S_0 is plotted vs. NDVI for 3 ranges of API. The main observations from these plots are:

- The sensible heat flux decreases with increasing NDVI in a slightly nonlinear fashion. Most rapid change of S_0 occurs near the middle range of NDVI with smaller rates of change for small (.2) and large (.6) NDVI. This expected asymptotic behavior at low and high NDVI results from the heat transfer being dominated by the soil surface and the canopy top, respectively.
- For small values of NDVI, most of the data points are in the small range of API (< 2.5 mm). In general, the data points for small (< 2.5mm) and high (18-22mm) values of API fall within 1-2 S_0 units of their corresponding curves (1 mm and 20 mm). However, data from the middle range of API (8.5-11.5) exhibit more scatter (2-3 S_0 units) about the mean.

Fig. 8 gives S_0 as a function of API for 3 ranges of NDVI. The following can be concluded from these plots:

- For large NDVI (.6), the sensible heat is insensitive to API. Values of S_0 range from 1-3 units.
- In the small range of NDVI (.1-.3), the sensible heat decreases with increasing API. The decrease is about a factor of 2 from low to moderate values of API. The scatter in S_0 is around 2 units, with increasing scatter as API increases.
- For the middle range of NDVI (.3-.5), there is also a strong trend toward decreasing sensible heat flux with API. In this case, the scatter of S_0 goes from 7 units at API near zero to 1 unit for API greater than 40mm.

It should be stressed that the indices, NDVI and API, are obtained independently from the measurement quantities (DT, and DH) used in the computation of S_0 . The correlations found here emanate from a relation of NDVI and API to physical processes governing the partitioning of energy at the surface. With proper scaling of S_0 for day to day variations in net radiation (R_n), Equation 10 could form the basis for estimation of sensible heat flux from measurements of NDVI and API with uncertainties of the magnitude cited here. The dependence of S_0 on R_n is presented in the following

sections. The quantitative link of S_0 to API appears to be the most tenuous. This is to be expected, however, given the uncertainty in the precipitation measurements and conversion to soil moisture used in the API calculations. Future improvements in remote measurements of near surface soil moisture from techniques such as active radars may yield improved relationships for the surface energy budget.

e. Comparison to Other Proposed Relationships.

The simple dependencies given by equations 7-10 are compared to two different semi-empirical models relating sensible heat to NDVI and API.

i. Heterogeneous Vegetation Cover

The first approach assumes that the NDVI is a measure of fractional vegetation cover and the partition between bare soil and canopy within a given grid cell. Following the approach of Chang and Wetzel (1991), the sensible heat flux can be written:

$$S_0 = (1-P)S_{bs} + P*S_{can} , \quad (11)$$

where S_{bs} and S_{can} are the heat flux from bare soil and the vegetative canopy, respectively. P is the fractional coverage of vegetation. Assuming a functional form of the fractional vegetative cover in terms of NDVI:

$$P = A*NDVI + B, \quad (12)$$

where A and B are constants.

Expressing S_{bs} in terms of sensible heat flux from wet and dry bare soil:

$$S_{bs} = (C)S_{bs}(\text{wet}) + (C^*-C)S_{bs}(\text{dry}) \quad (13)$$

Relating the coefficients b and b^* to volumetric soil moisture, we assume a non-linear increase of b approximated by a cubic change with soil moisture (Wetzel et al., 1984):

$$C = a_3 * (w/w_s)^3 \quad (14)$$

$$C^* = a_3 * (w_{max}/w_s)^3 ,$$

where (w/w_s) and (w_{max}/w_s) are the volumetric and maximum volumetric soil moisture. Furthermore, the volumetric soil moisture is a linear function of API;

$$(w/w_s) = D * API + E, \quad (15)$$

where D and E are constants.

For testing purposes here, $S_{bs}(\text{wet})$ and $S_{bs}(\text{dry})$, when normalized by surface net radiation (R_n), are assumed constant over the domain for a particular day. In reality, these are functions of soil type and atmospheric conditions such as wind speed and humidity which can vary over the domain. Using the relation for sensible heat flux over the canopy given by Norman et al. (1995),

$$S_{can} = R_n * [1 - 1.3f_g (\Delta + \gamma)] \quad (16)$$

where f_g is the fraction of canopy which is green (assumed to be unity), γ is a constant (.066 kPa/deg K), γ is the rate of change of saturation vapor pressure with temperature (a function of temperature). As the temperature increases, S_{can} decreases. As a first assumption, we neglect any variation in daytime mean temperature across the domain. In this case, S_{can} is taken as a constant on a given day.

Rewriting (11) and combining constants, we obtain an equation for S_0 (normalized by R_n) of the following form,

$$S_0 = a_0 + a_1 * API^3 + a_2 * API^2 + a_3 * API + (a_4 * API^3 + a_5 * API^2 + a_6 * API) * NDVI + a_7 * NDVI, \quad (17)$$

where the constants a_0 through a_7 are scaled by R_n .

In summary, (17) is based on the NDVI being a measure of fractional vegetation cover and a partition between bare soil and canopy. The normalized heat flux over the canopy is based on empirical relations which are a function of air temperature. The change from dry to wet soil flux is modeled to be non-linear (cubic) with soil moisture. As a result of the use of these relations, the

form of (17) differs from the ad-hoc version (10) in that it includes a cubic term for API, only a linear term for NDVI, and cross terms of API times NDVI.

Multiple linear regression was applied to our data set to derive the coefficients in (17). Results are summarized in Table 5a.

TABLE 5a. Regression statistics for the heterogeneous vegetation model: S_0 versus NDVI and API.

Date	a_0	a_1	a_2	a_3	a_4	a_5	a_6	a_7	r	rms
26 May	12.28	.00015	-.0102	-.0062	.0003	-.0250	.1698	17.82	.914	1.116
27 May	14.54	-.0002	.0211	-.640	-.0004	.0345	-1.104	22.75	.881	1.751

Overall, the correlation is slightly higher and the rms is slightly lower than for Eq.(10) on both days. The best fit curves are plotted in Figs. 9 and 10 for different constant values of API and NDVI, respectively. The dependence of S_0 on NDVI is basically linear and does not capture the slight inflections in the scatter plots at low and high NDVI. As compared to the results of Eq. 10, the slope of S_0 vs. NDVI changes more between low and high API: the slope becomes more negative for smaller API. Also, the slope of the S_0 vs. API curves changes more between high and low NDVI. This slope becomes more negative for smaller NDVI. Both of these effects appear to be reflected in the data.

Next, point to point variations in temperature were considered in (16). This leads to inclusion of 2 additional terms in (17), $a_8 \cdot \text{NDVI} \cdot S_{\text{can}} + a_9 \cdot S_{\text{can}}$. The mean daytime temperature at each grid point was obtained by averaging the maximum and minimum temperature interpolated from the Cooperative surface stations. This temperature was used to evaluate S_{can} . The multiple regression including the extra terms in (17) was performed and the results are given in Table 5b.

TABLE 5b. Regression statistics for the heterogeneous vegetation model: S_0 versus NDVI and API including temperature.

Date	a_0	a_1	a_2	a_3	a_4	a_5	a_6	a_7	a_8	a_9	r	rms
26 May	12.00	.00011	-.0080	-.0218	-.0003	-.0205	.1419	18.05	8.340	12.37	.922	1.019
27 May	13.79	-.0002	.0188	-.540	-.0004	.0303	-.898	21.66	19.26	-8.31	.896	1.534

A modest increase in the correlation and decrease in the rms is observed, however the changes are not considered significant given the inclusion of additional terms.

ii. Homogeneous Vegetation Cover

This approach assumes uniform coverage of vegetation within a sampling cell. The NDVI is then a measure of canopy thickness. In this case, Eq. 11 is replaced by,

$$S_0 = \Delta R_n * S_{can} + (1 - \Delta R_n) * S_b \quad (18)$$

where ΔR_n is the net radiation absorbed by the canopy. Following Norman et al. (1995), this term is given by:

$$\Delta R_n = R_n (1 - \exp(0.9 * \ln(1 - f_c))), \quad (19)$$

where f_c is the canopy cover, and is related to the Leaf Area Index (LAI) by:

$$f_c = 1 - \exp(-.5 * LAI) \quad (20)$$

Using the empirical relation between LAI and NDVI from (Kustas et al., 1993a) in (20),

$$f_c = 1 - [(.9 - NDVI) / .774]^{-.361}, \quad (21)$$

where the constant .9 is considered an upper limit for NDVI.

Substituting (13), (19) and (21) into (18), we obtain,

$$S_0 = a_0 + a_1 * F * API^3 + a_2 * F * API^2 + a_3 * F * API + a_4 * F, \quad (22)$$

where,

$$F = [(.9-NDVI)/.774]^{-397}, \quad (23)$$

and the constants a_0 through a_4 are scaled by R_n .

Multiple linear regression was again used to determine the coefficients in Eq. (22). Results are summarized in Table 6a.

TABLE 6a. Regression statistics for the homogenous vegetation model: S_0 versus NDVI and API.

Date	a_0	a_1	a_2	a_3	a_4	r	rms
26 May	-16.90	-.00003	.00469	-.192	26.57	.903	1.256
27 May	-18.61	-.00012	.0123	-.324	28.92	.866	1.948

Overall, the correlation is slightly lower and the rms is slightly higher than for the heterogeneous method on both days. These values are quite similar to those obtained with the regressions from Eq. 10. The best fit curves are plotted in Figs. 11 and 12 for constant API and NDVI, respectively. The dependence of S_0 on NDVI is nonlinear but appears to curve in the opposite sense from the data and best fit curves from Eq. 10 (Fig. 11). As with the curves resulting from Eq. 10, the slope of S_0 vs. NDVI is roughly invariant between low and high API. Also, the slope of the S_0 vs. API curves exhibits little change between high and low NDVI.

The effect of point to point variations in daytime temperatures were considered in the same manner as presented for the heterogeneous method. In this case, 2 additional terms are added to (22), $a_5 * S_{can} - a_6 * S_{can} * F$. The results of the multiple regression including these terms are given in Table 6b.

TABLE 6b. Regression statistics for the homogenous vegetation model: S_0 versus NDVI and API including temperature effects.

Date	a_0	a_1	a_2	a_3	a_4	a_5	a_6	r	rms

26 May	-20.91	-.00003	.00408	-.175	30.43	113.7	108.5	.915	1.11
27 May	-20.54	-.00009	.00997	-.277	30.52	76.56	62.64	.887	1.66

As with the heterogeneous method, modest improvements in the correlation and rms are observed when including the temperature. However, the explained variance does not decrease significantly. In general, it appears that the heterogeneous method produces a slightly superior fit to the data than the homogenous vegetation model and the simple polynomial approach.

f. Microwave-Based API Comparisons

The microwave-based API was evaluated from SSM/I data on 26 May 1991 following the simple ratio technique and the dynamic database technique described in Section 1. Application of the latter technique utilized data from the previous 2 days as well.

i. Ratio Technique

Correlations made with ground based API are very small on this day over the domain of interest. It appears that there is little useful information in the SSM/I data using this technique on 26 May 1991. The reasons for this are unclear at this time.

ii. Dynamic Database

It was found that little information was contained in this dataset. API_m values were mainly zero over the entire domain as the technique considered soil moisture values to be below a minimum detectable threshold at many points. Apparently, surface moisture was generally too small for useful application of the SSM/I data in this case.

g. Conclusions

Using a simple slab boundary layer model and optimal estimation interpolation, GOES infrared surface temperature data and rawinsonde observations were interpreted to produce sensible heat flux estimates for the Texas/Oklahoma area during the presence of a dry-line. The spatial distribution of sensible heat flux reflects the general west-east gradient in vegetation cover (NDVI) across the region. However, the gradient does not appear to be locally more intense in vicinity to the

atmospheric dry-line feature. This is probably realistic given the land cover distribution in the area. The north-south irregularity in NDVI across the Texas Panhandle, proposed by Hane et al. (1997) to locally alter the eastward extent of the dry-line and to influence convective storm initiation, is undetected by this analysis. Scattered cloud cover nearby the feature and its small-scale compared to analysis resolution are limiting factors in detection.

Several factors may limit the accuracy of the regressions presented in Sects. 4d-e in predicting the normalized heat flux. Spatial variability in the atmosphere and soil characteristics have not been taken into account in the values of canopy and bare soil heat flux (wet and dry). Moreover, the use of NDVI as a measure of LAI has limitations. The NDVI reaches a maximum for moderately large LAI and can not distinguish larger values. Moreover, the exact relationship with LAI is dependent on vegetation type. These factors can account for some of the difference observed in the best fit of (17) and (22). More importantly, the same uncertainties in API which are discussed in section 4d limit the correlations here. Without a more precise measure of surface soil moisture, the added sophistication of the partitioning between wet and dry soil cannot be adequately tested.

Unlike in the Midwest case presented in Section 3, the passive microwave derived API from SSM/I data did not provide useful estimates of surface wetness as compared to ground based API. It is believed that the dynamic range of surface wetness was too small given large changes of vegetation cover across the region to extract a meaningful signal from the microwave brightness temperatures. Additional work may be required to more fully explore the deficiencies in the SSM/I data for this case.

In order to consider applying the equations (10), (17) and (22) on days or locations with different amounts of daytime net radiation, the coefficients in these equations must be multiplied by $R_n/R_n(0)$, where $R_n(0)$ is 17.5 MJm^{-2} in the case of 26 May and 18.0 MJm^{-2} in the case of 27 May. The regression equations should be tested against other cases in order to further demonstrate the validity in other conditions.

5. Other Related Research

The effects of surface wetness on the potential for deep convection was evaluated through scaling, modeling, and observations in Segal et al. (1995). Some empirical approaches using satellite

data to estimate mesoscale surface fluxes of heat and moisture were reviewed. It was found that in general increasing surface wetness has the effect of increasing the thermodynamic instability required for deep convection with strong updrafts.

References

- Carlson, T. N., R. R. Gillies and E. Perry, 1993: A method to make use of thermal infrared temperature and NDVI measurements to infer surface soil water content and fractional vegetation cover. Accepted for publication in *Remote Sensing Reviews*.
- Chang, J.-T., and P.J. Wetzel, 1991: Effects of spatial variations on soil moisture and vegetation on the evolution of a prestorm environment: A numerical case study. *Mon. Wea. Rev.*, 119, 1368-1390.
- Diak, G. R. and T. R. Stewart, 1989: Assessment of surface turbulent fluxes using geostationary satellite surface skin temperature and a mixed layer planetary boundary layer scheme. *J. Geophys. Res.*, 94, 6357-6373.
- Diak, G. R., and M. W. Whipple, 1993: Improvements to models and methods for evaluating the land-surface energy balance and "effective" roughness using radiosonde reports and satellite-measured "skin" temperatures. *J. Ag. For. Meteor.*, 63, 189-218.
- Diak, G.R., M.W. Whipple, 1994: A note on the use of rawinsonde data to estimate the daytime fluxes of sensible and latent heat: a comparison with surface flux measurements from the FIFE. *J. Ag. For. Meteor.*, 68: 63-75.
- Diak, G.R., M.W. Whipple, 1995: Note on estimating surface sensible heat fluxes using surface temperatures measured from a geostationary satellite during FIFE 1989. *J. Geophys. Res.*, 100, No. D12: 25453-25461.
- Driedonks, A. G. M., 1982a: Sensitivity analysis of the equations for a convective mixed layer. *Boundary Layer Meteorol.*, 22, 475-480.
- Driedonks, A. G. M., 1982b: Models and observations of the growth of the atmospheric boundary layer. *Boundary Layer Meteorol.*, 23, 284-306.
- Garratt, J. R. and B. B. Hicks, 1973: Momentum, heat and water vapour transfer to and from natural surfaces. *Q. J. Roy. Meteor. Soc.*, 99, 680-687.
- Gillies, R. R., T. N. Carlson, J. Cui, W. P. Kustas and K. S. Humes, 1997: A verification of the 'triangle' method for obtaining surface soil water content and energy fluxes from remote measurements of the Normalized Difference Vegetation Index (NDVI) and surface radiant temperature. *Int. J. Remote Sensing*, 18, 3145-3166.
- Hane, C.E., H.B. Bluestein, T.M. Crawford, M.E. Baldwin, R.M. Rabin, 1997: Severe thunderstorm development in relation to along-dryline variability: A case study. *Mon. Wea. Rev.*, 125, 231-251.
- Kustas, W. P., C. S. T. Daughtry and P. J. Van Oevelen, 1993a: Analytical treatment of the relationships between soil heat flux/net radiation ratio and vegetation indices. *Remote Sens. Envir.*, 46, 319-330.

- Kustas, W. P., T. J. Schmugge, K. S. Humes, T. J. Jackson and R. Parry, 1993b: Relationships between evaporative fraction and remotely sensed vegetation index and microwave brightness temperature for semiarid rangelands. *J. Appl. Meteor.*, 32, 1781-1790.
- Moran, M. S., 1990: A satellite-based approach for evaluation of the spatial distribution of evapotranspiration from agricultural lands, Ph.D Diss., Univ. of Ariz., Tucson, AZ, 223 pp.
- Neale, C. M. U., M. J. McFarland and K. Chang 1990: Land surface type classification using microwave brightness temperatures from the Special Sensor Microwave/Imager. *IEEE Trans. Geosci. Remote Sensing*, 28, 5, 829-838.
- Nemani, R., L. Piers and S. Running, 1993: Developing satellite-derived estimates of surface moisture status. *J. Appl. Meteor.*, 32, 548-557.
- Norman, J. M., C., M. Divakarla and N. Goel, 1993: Algorithms for extracting information from remote thermal-ir observations of the earth's surface. Accepted for publication, *Rem. Sens. Env.*
- Norman, J. M., W. P. Kustas, K. S. Humes, 1995: Source approach for estimating soil and vegetation energy fluxes in observations of directional radiometric surface temperature. *J. Ag. For. Meteor.*, 77, 263-293.
- Oke, T. R., 1978: Boundary Layer Climates, New York, John Wiley & Sons, 372pp.
Geosci. Remote Sensing, GE-18, 353-361.
- Wetzel, P. J., D. Atlas, and R. Woodward, 1984: Determining soil moisture from geosynchronous satellite infrared data: A feasibility study. *J. Clim. Appl. Meteor.*, 23, 375-391.

Figure Captions

Fig. 1. Spatial distribution of derived surface energy parameters: a) S_0 , b) B_0 , c) Z_0 . The satellite derived vegetation index, NDVI, is shown in the background.

Fig. 2. B_0 , vs. NDVI: a) 26 May 91, b) 27 May 91.

Fig. 3. B_0 , vs. API: a) 26 May 91, b) 27 May 91.

Fig. 4. Z_0 vs. NDVI: a) 26 May 91, b) 27 May 91.

Fig. 5. Z_0 vs. API: a) 26 May 91, b) 27 May 91.

Fig. 6. S_0 vs. a) DT_s , b) NDVI, c) API, d) DH.

Fig. 7. Simple polynomial model: S_0 vs. NDVI for different ranges of API: a) 26 May 91, b) 27 May 91.

Fig. 8. Simple polynomial model: S_0 vs. API for different ranges of NDVI: a) 26 May 91, b) 27 May 91.

Fig. 9. Heterogeneous vegetation model: S_0 vs. NDVI for different ranges of API: a) 26 May 91, b) 27 May 91.

Fig. 10. Heterogeneous vegetation model: S_0 vs. API for different ranges of NDVI: a) 26 May 91, b) 27 May 91.

Fig. 11. Homogeneous vegetation model: S_0 vs. NDVI for different ranges of API: a) 26 May 91, b) 27 May 91.

Fig. 12. Homogeneous vegetation model: S_0 vs. API for different ranges of NDVI: a) 26 May 91, b) 27 May 91.

List of Tables

Table 1. Regression statistics: S_0 vs. DT_s .

Table 2. Regression statistics: S_0 versus NDVI.

Table 3. Regression statistics: S_0 versus $\log(\text{API})$.

Table 4. Regression statistics: S_0 versus NDVI and API.

Table 5a. Regression statistics for the heterogeneous vegetation model: S_0 versus NDVI and API.

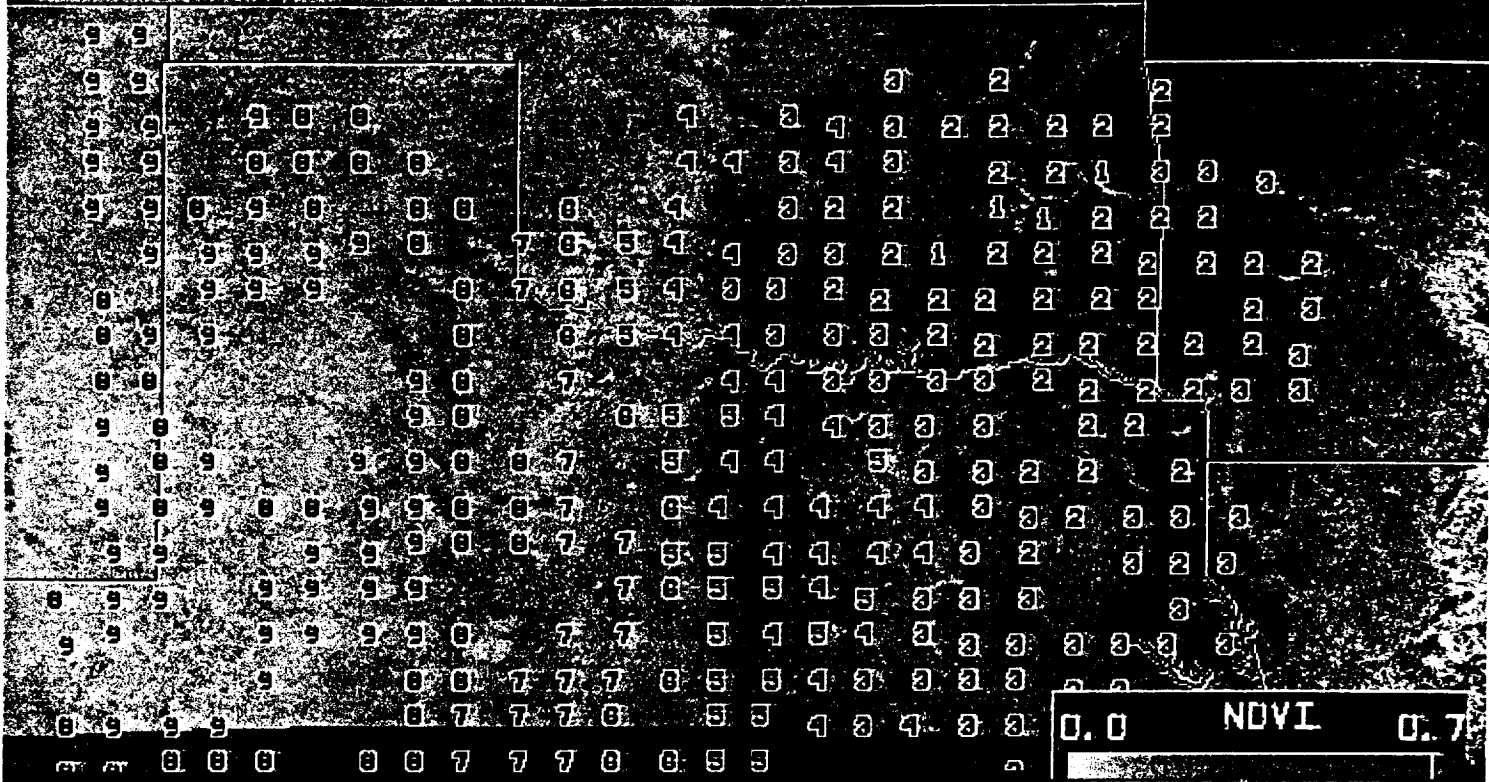
Table 5b. Regression statistics for the heterogeneous vegetation model: S_0 versus NDVI and API including temperature.

Table 6a. Regression statistics for the homogeneous vegetation model: S_0 versus NDVI and API.

Table 6b. Regression statistics for the homogeneous vegetation model: S_0 versus NDVI and API including temperature effects.

Fig. 1a

26 May 1991



27 May 1991

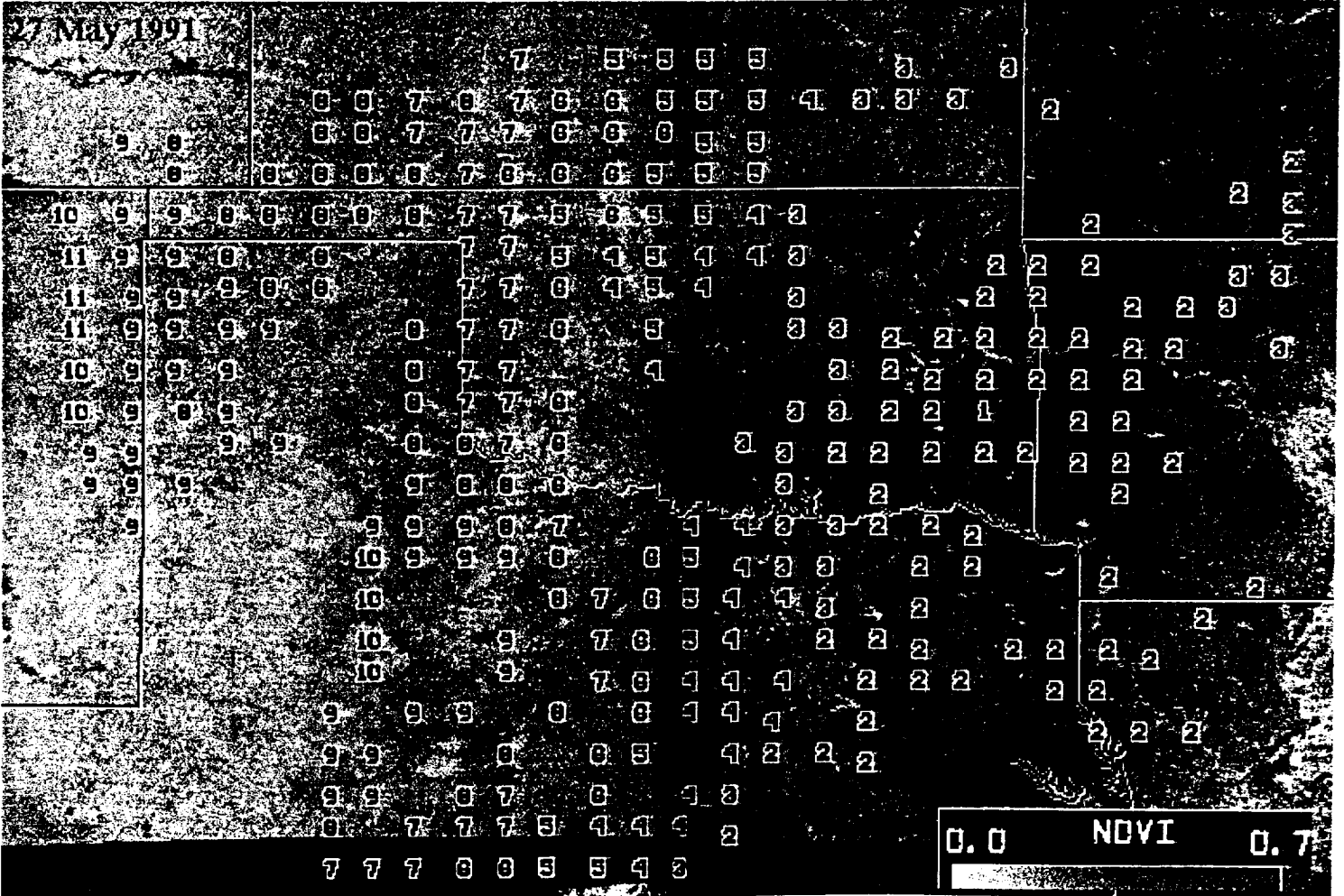
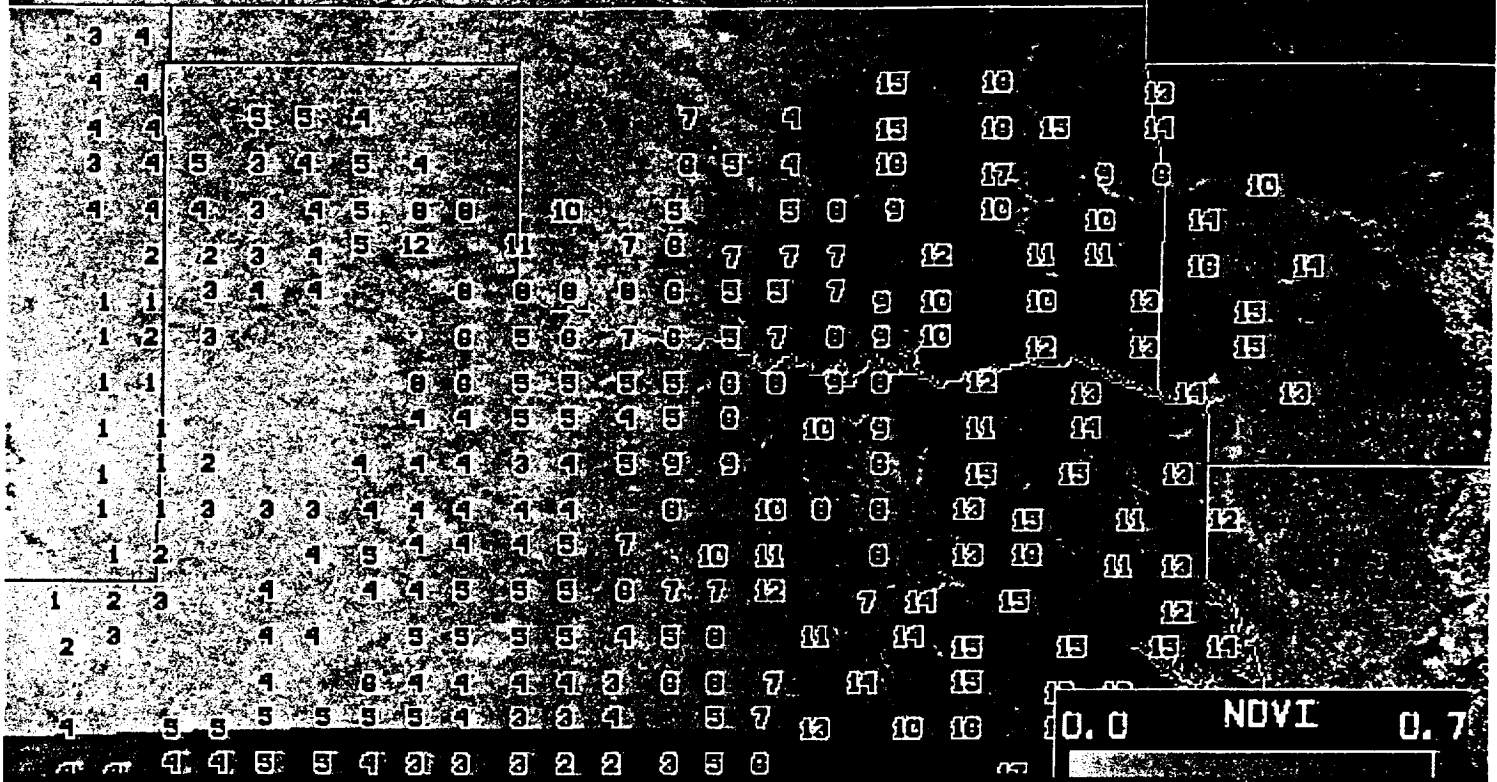


Fig. 1c

26 May 1991



27 May 1991

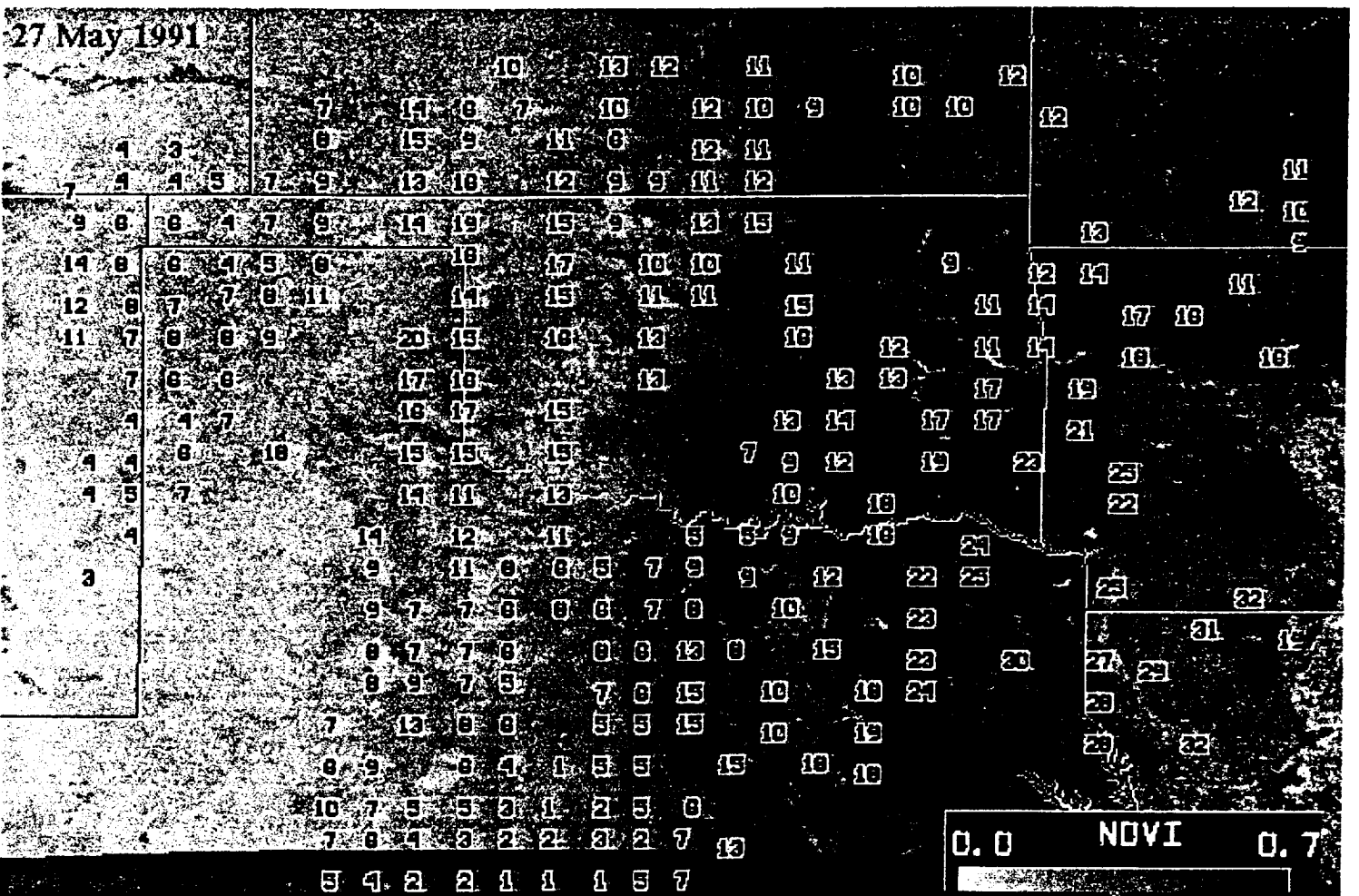


Fig. 2a

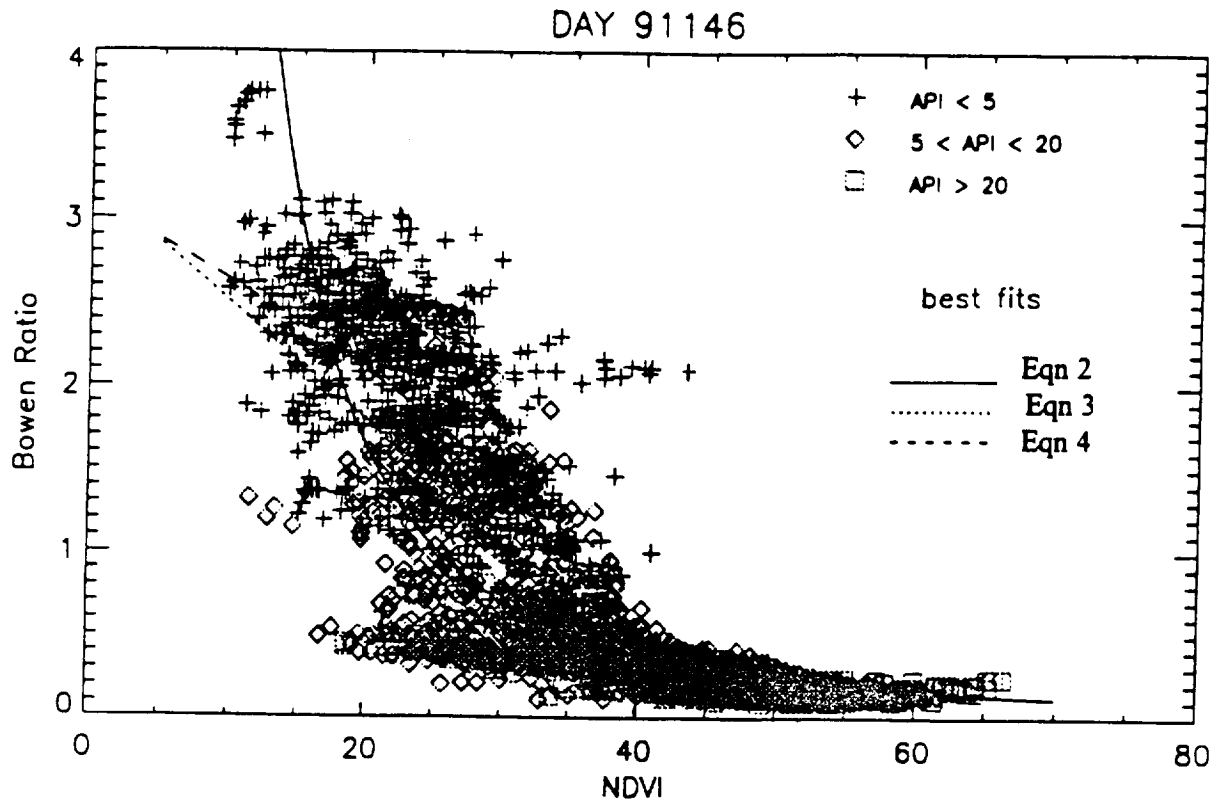


Fig. 2b

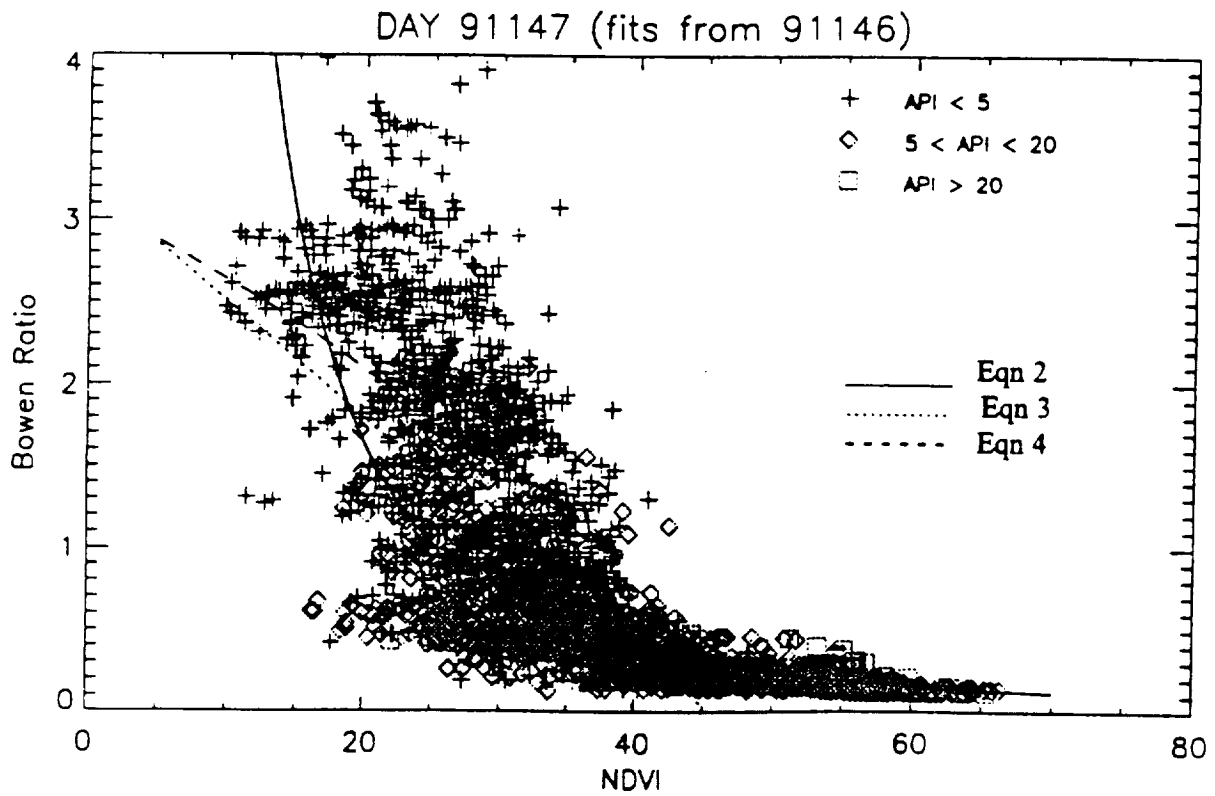


Fig. 3a

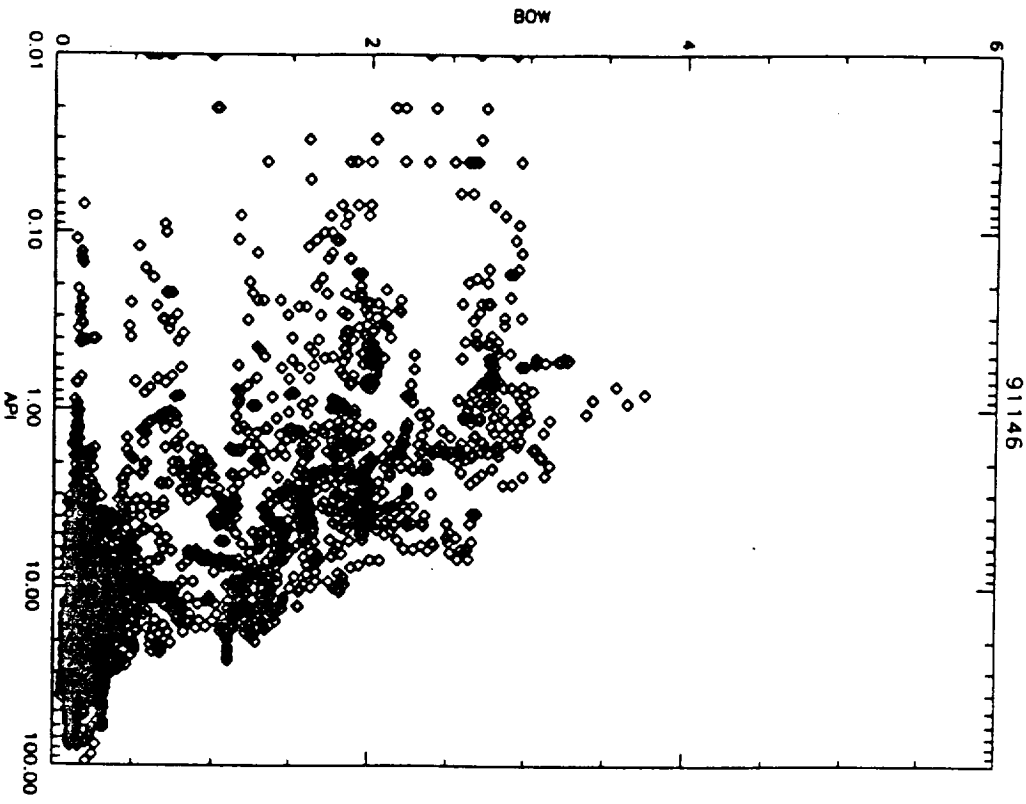


Fig. 3b

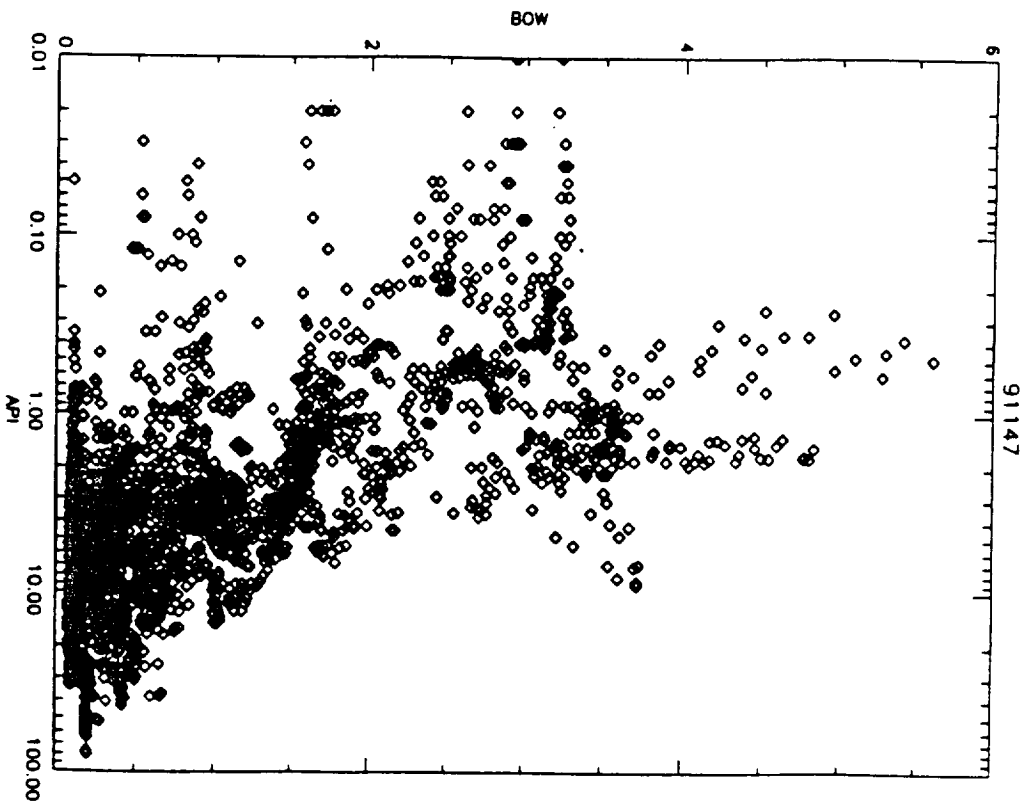


Fig. 4a

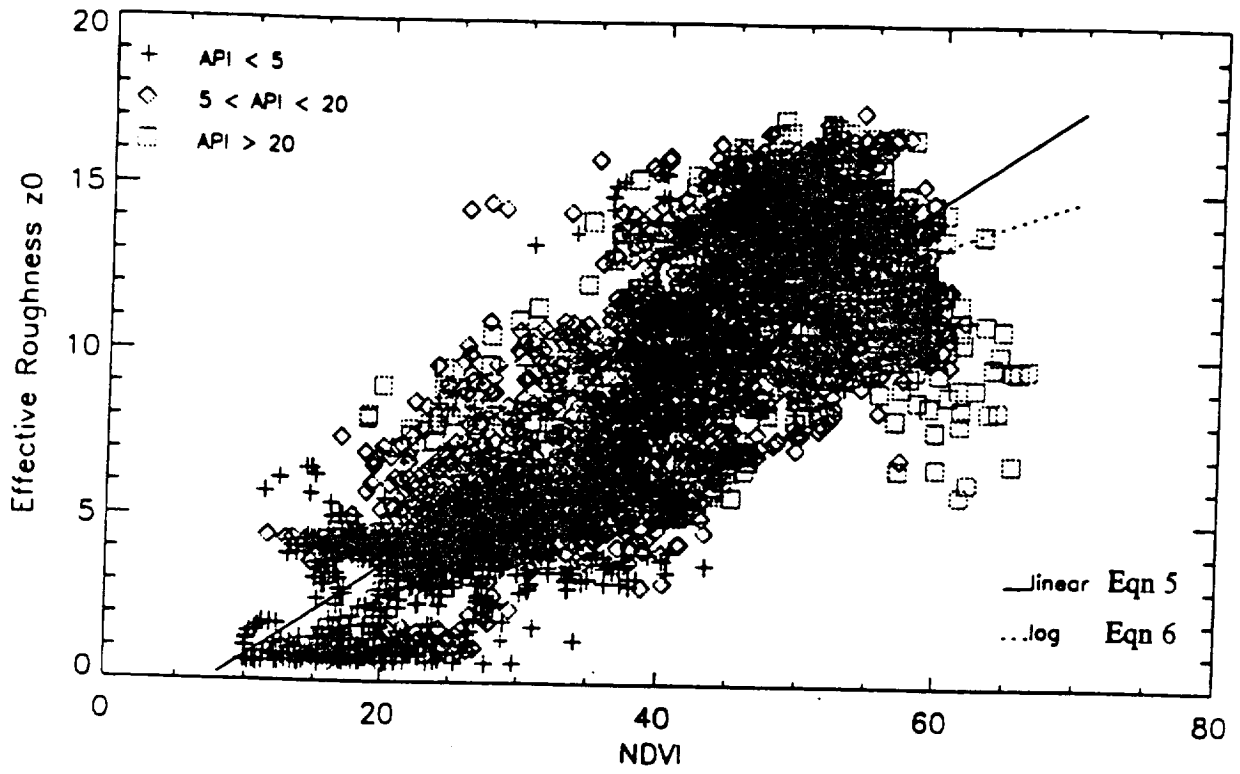


Fig. 4b

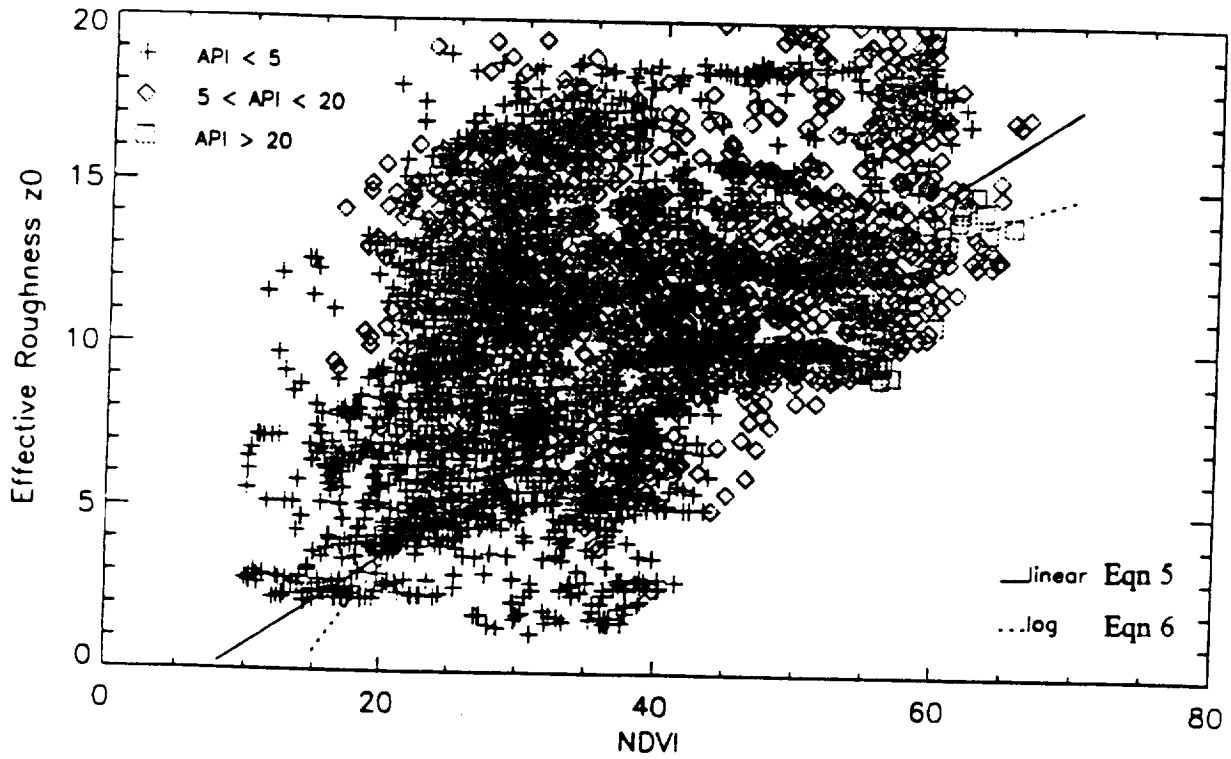


Fig. 5a

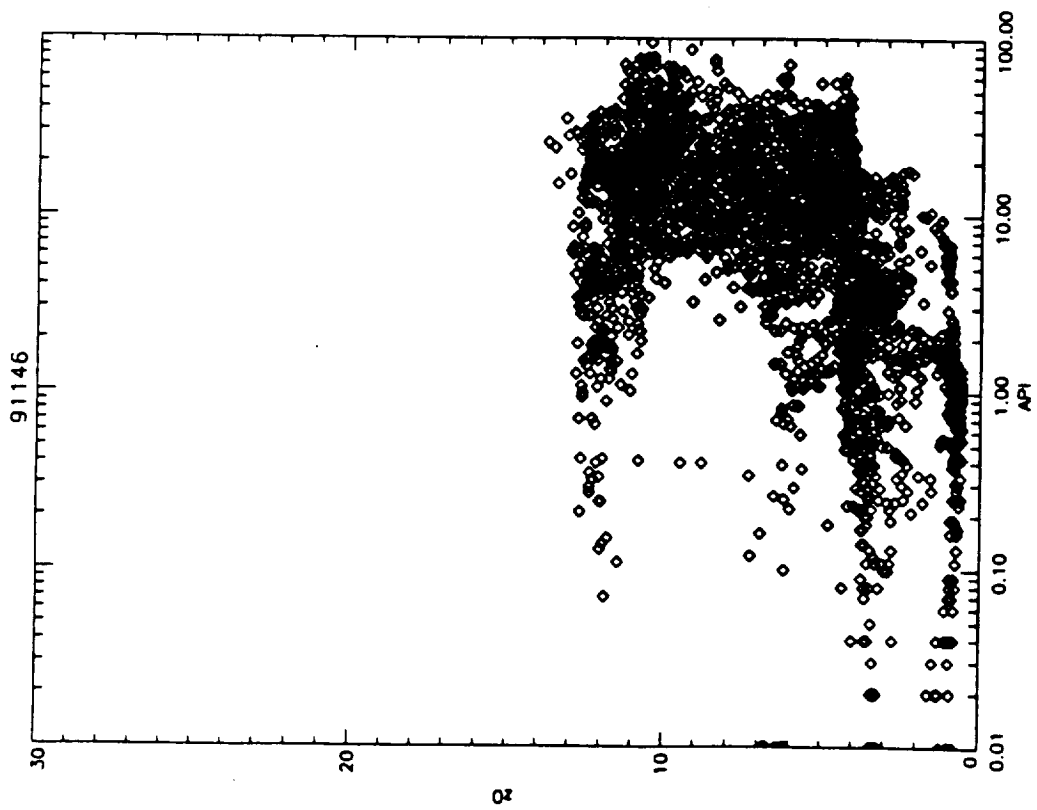


Fig. 5b

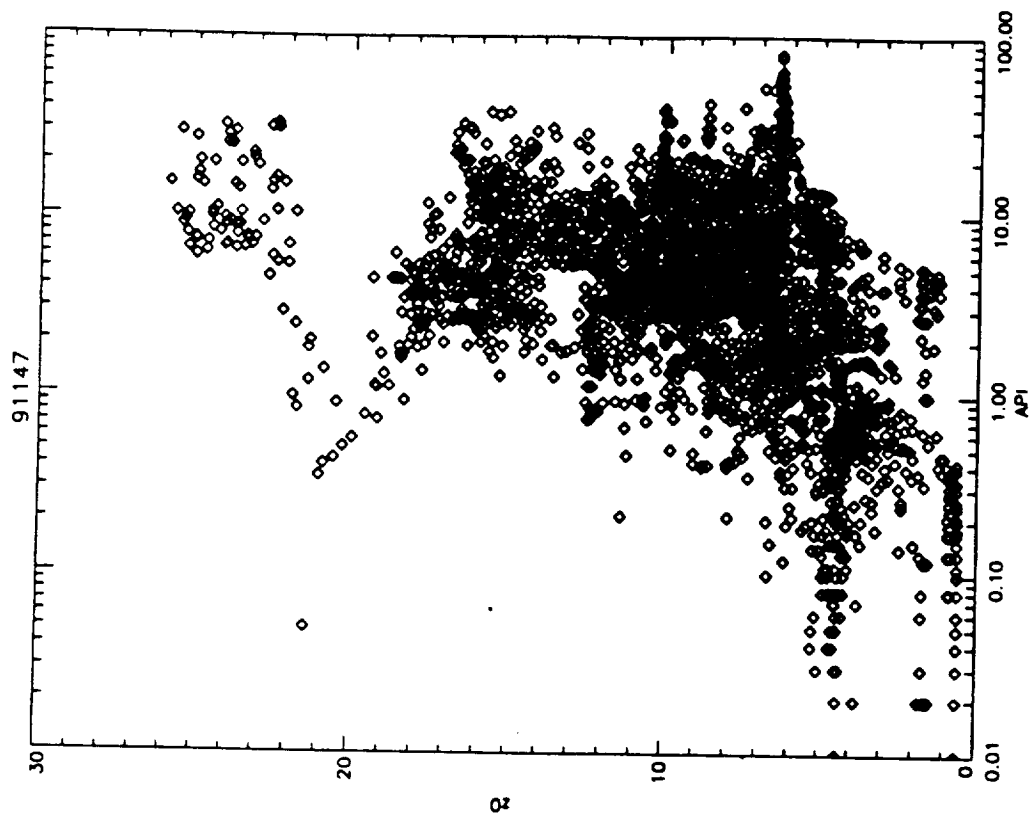


Fig. 6a

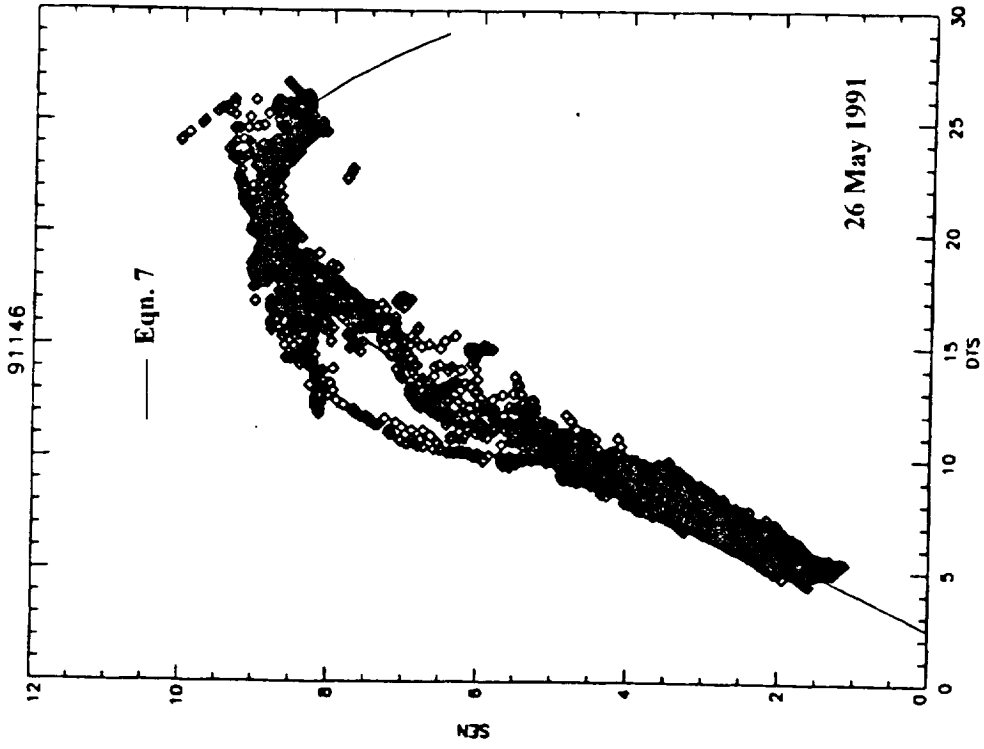
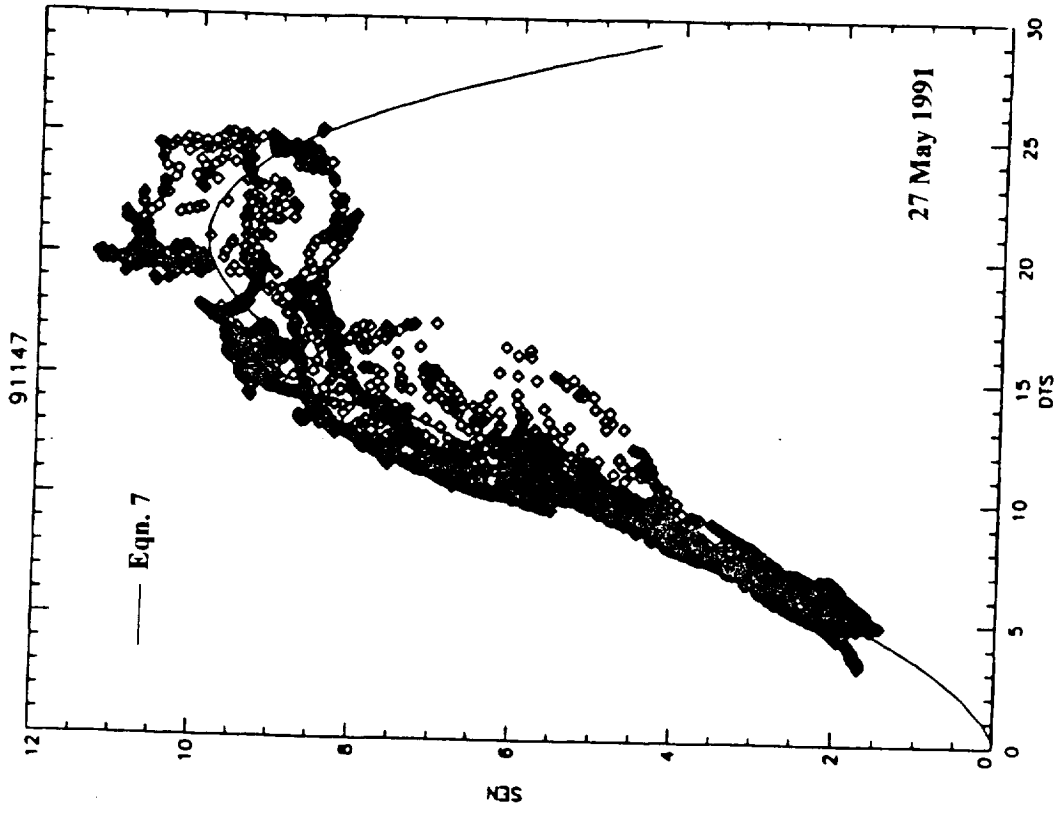


Fig. 6b

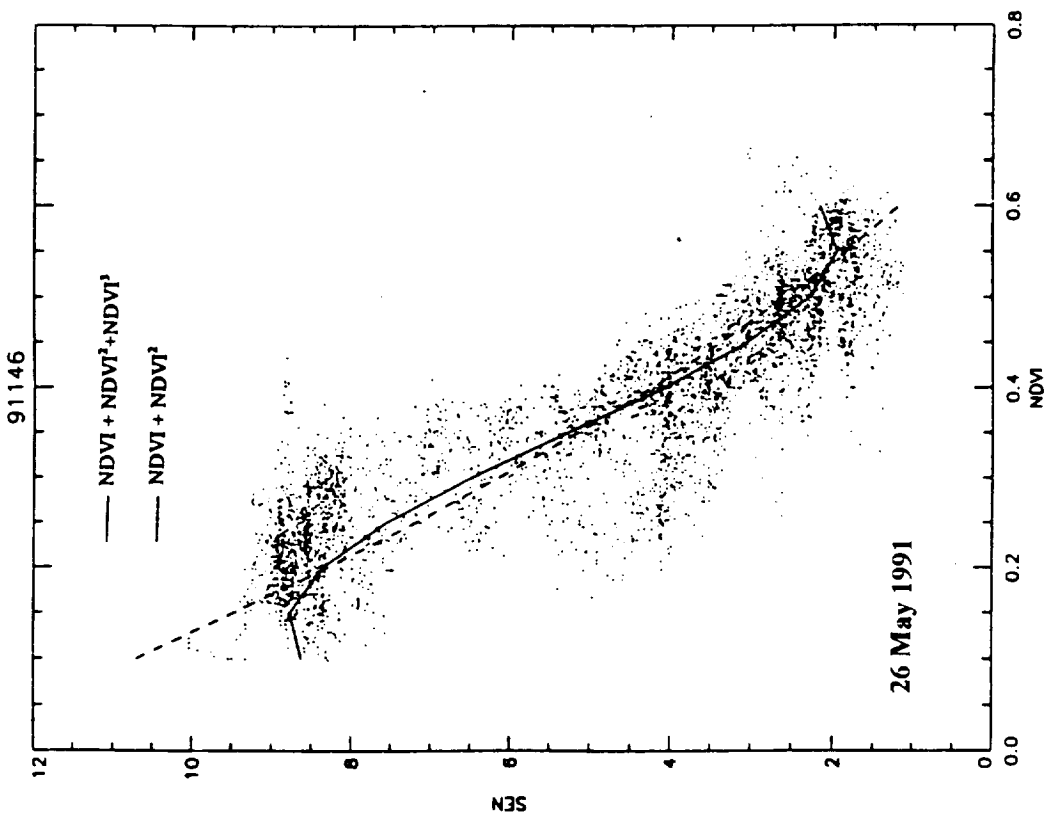
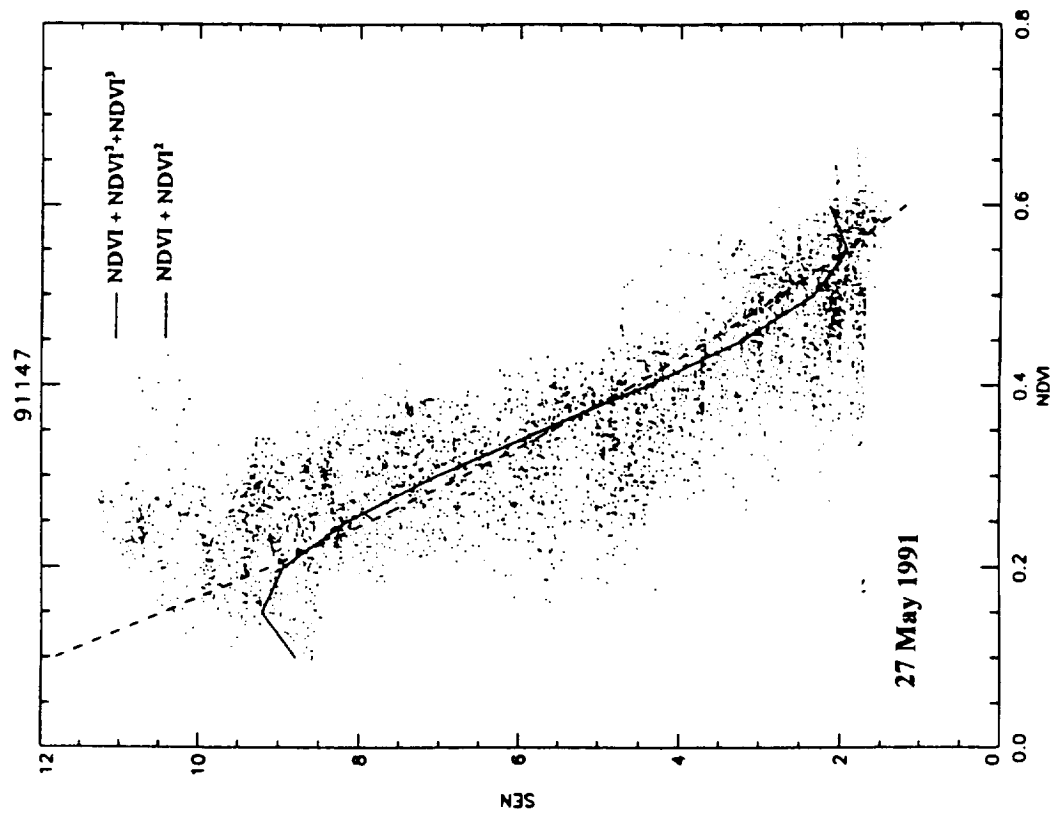


Fig. 6c

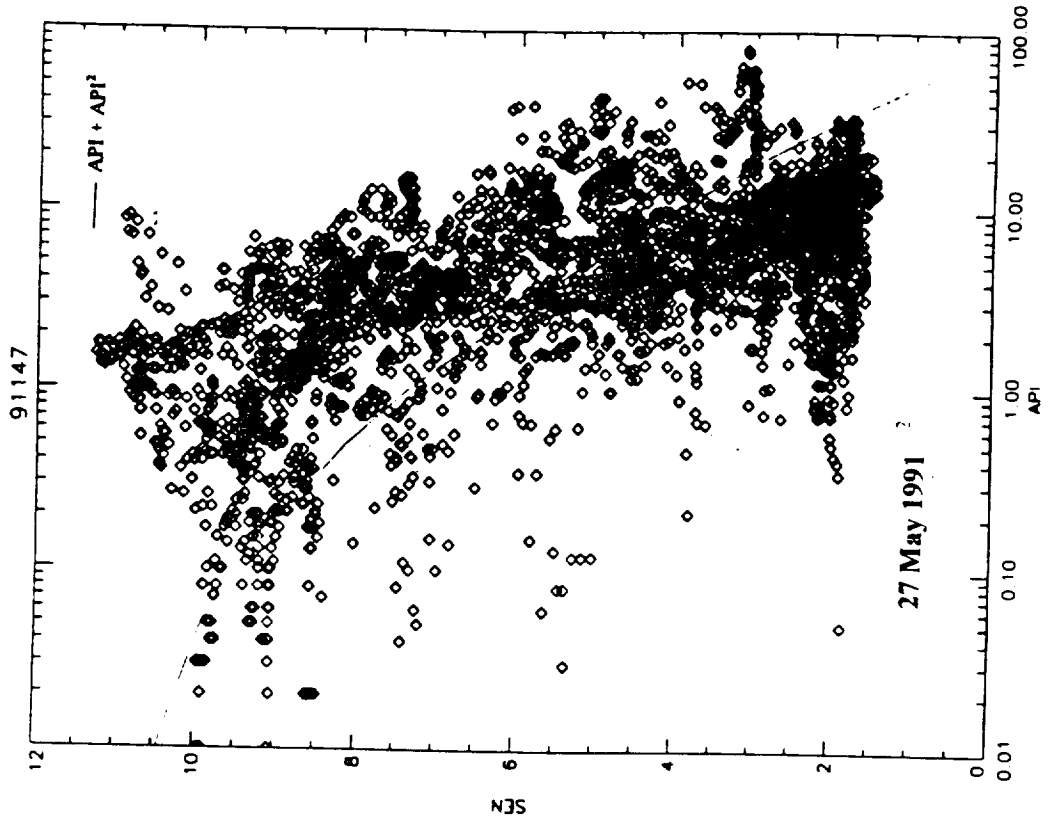
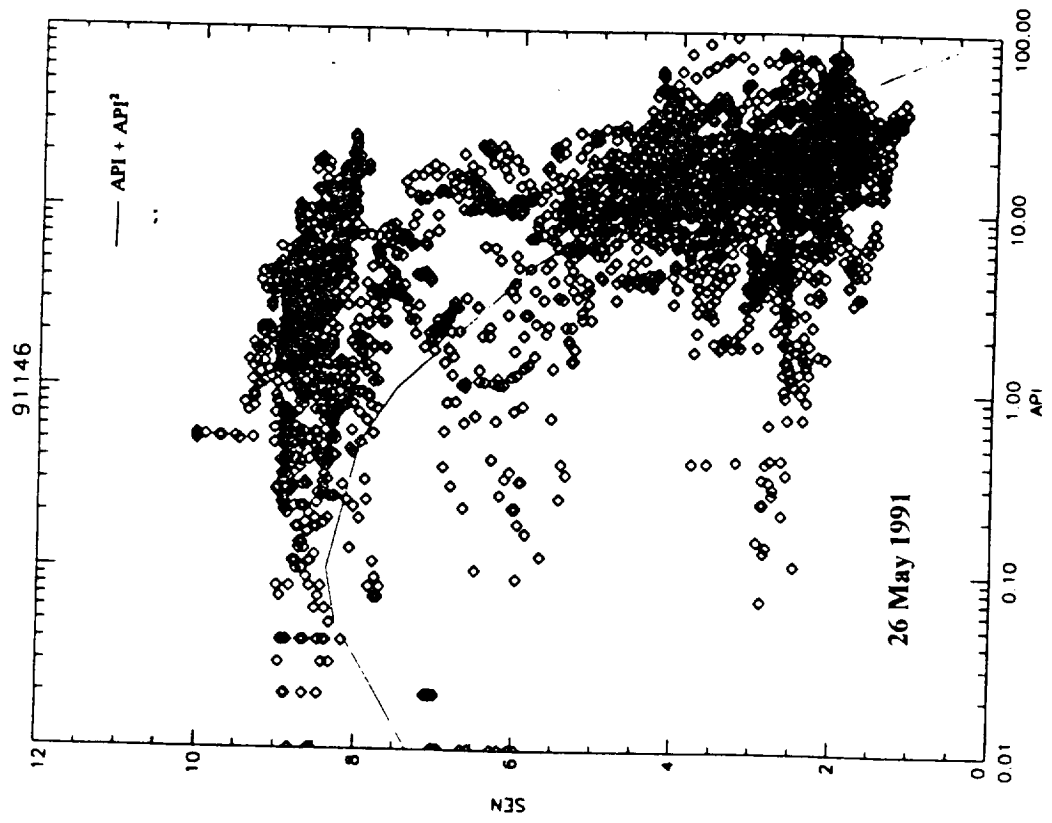


Fig. 6d

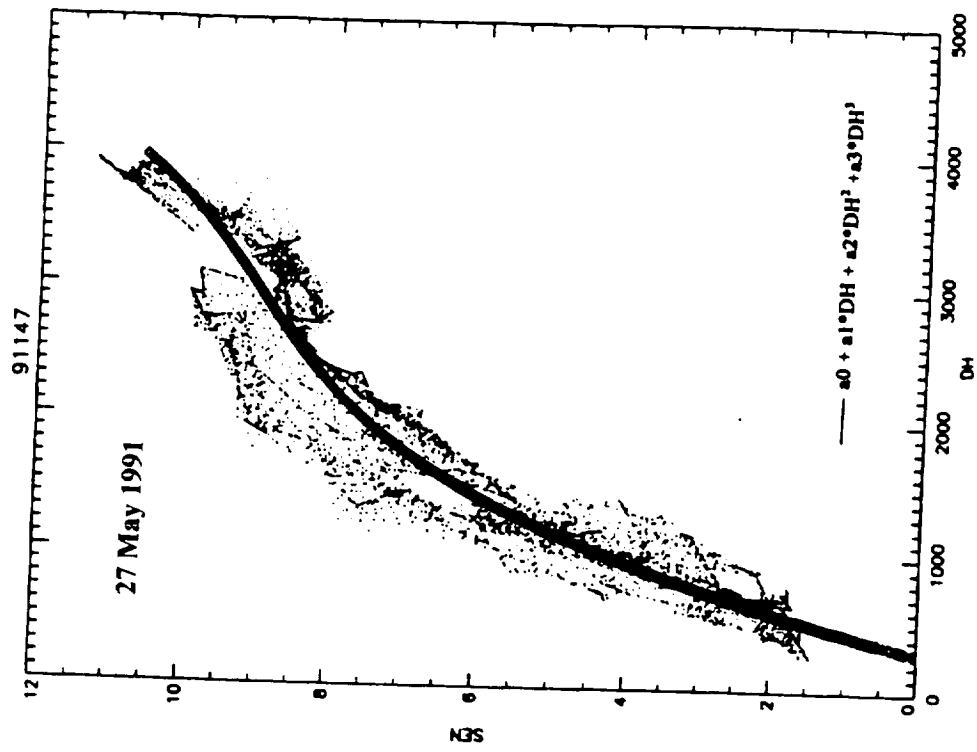
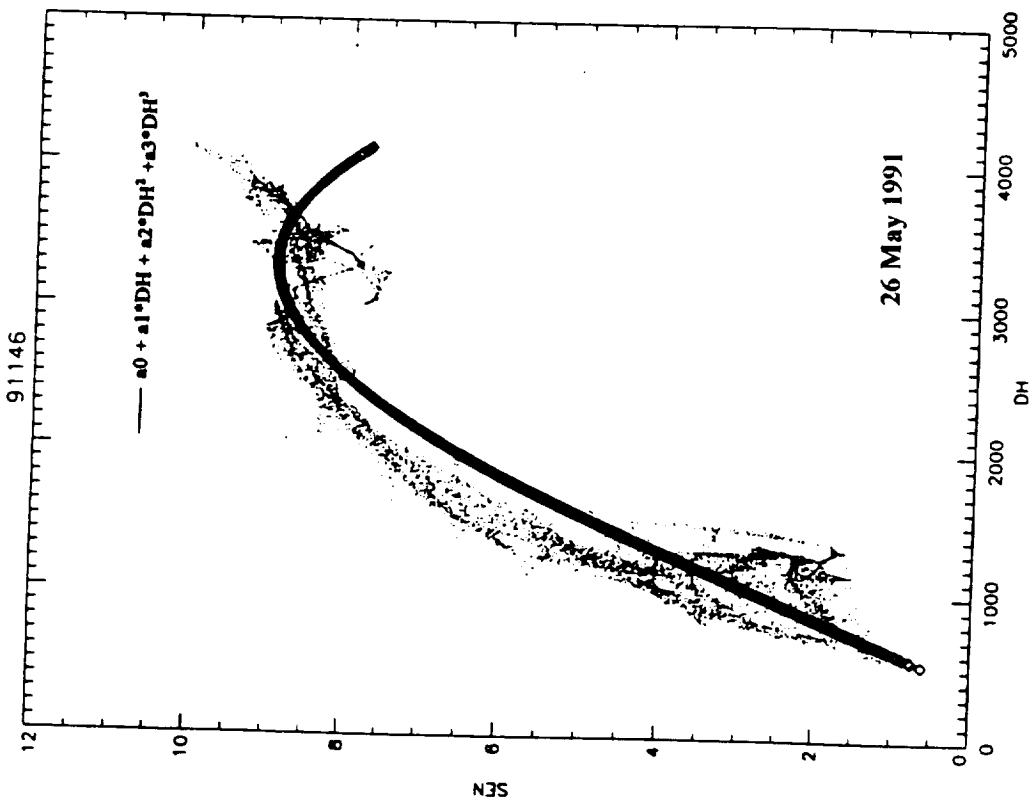


Fig. 7a

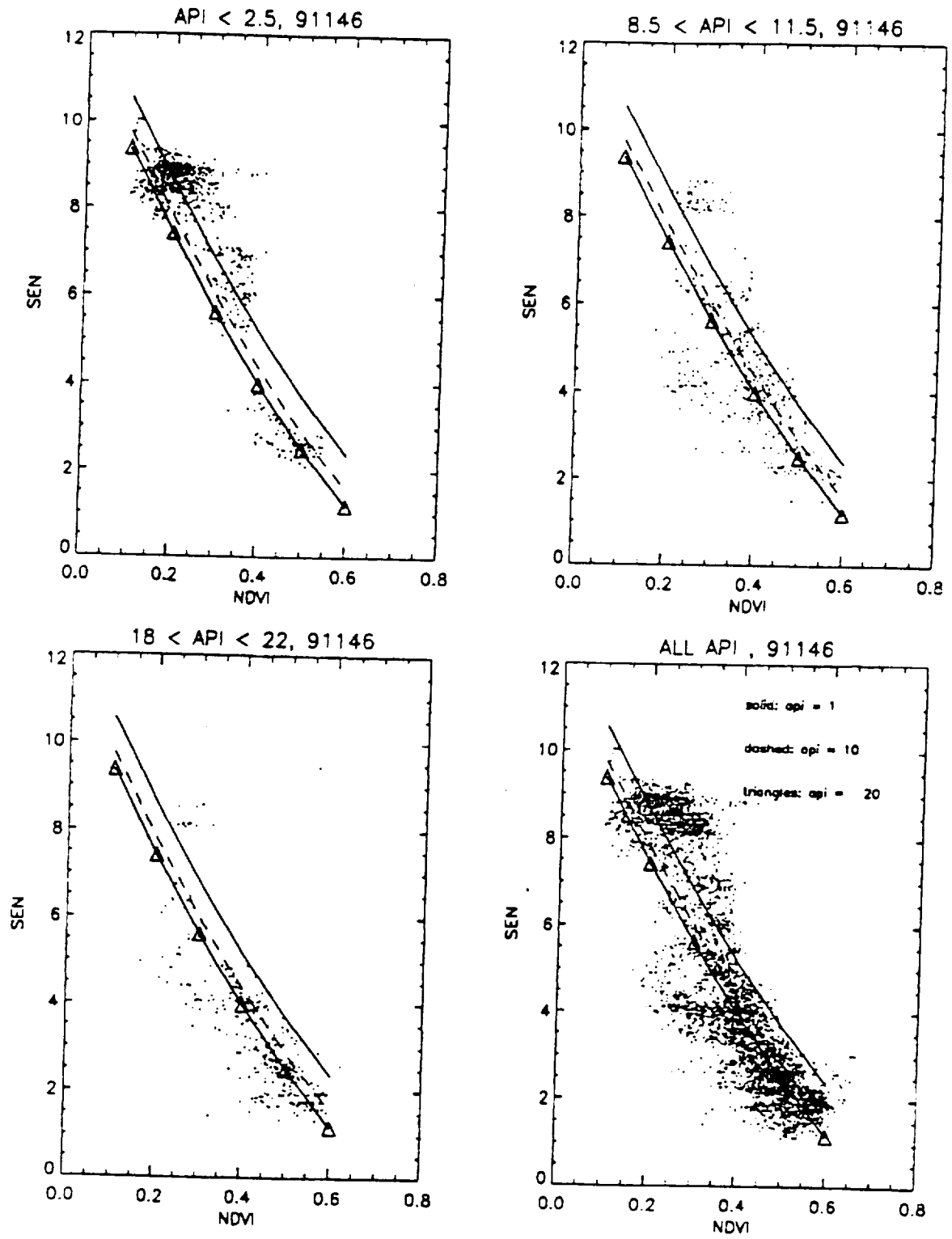


Fig. 7b

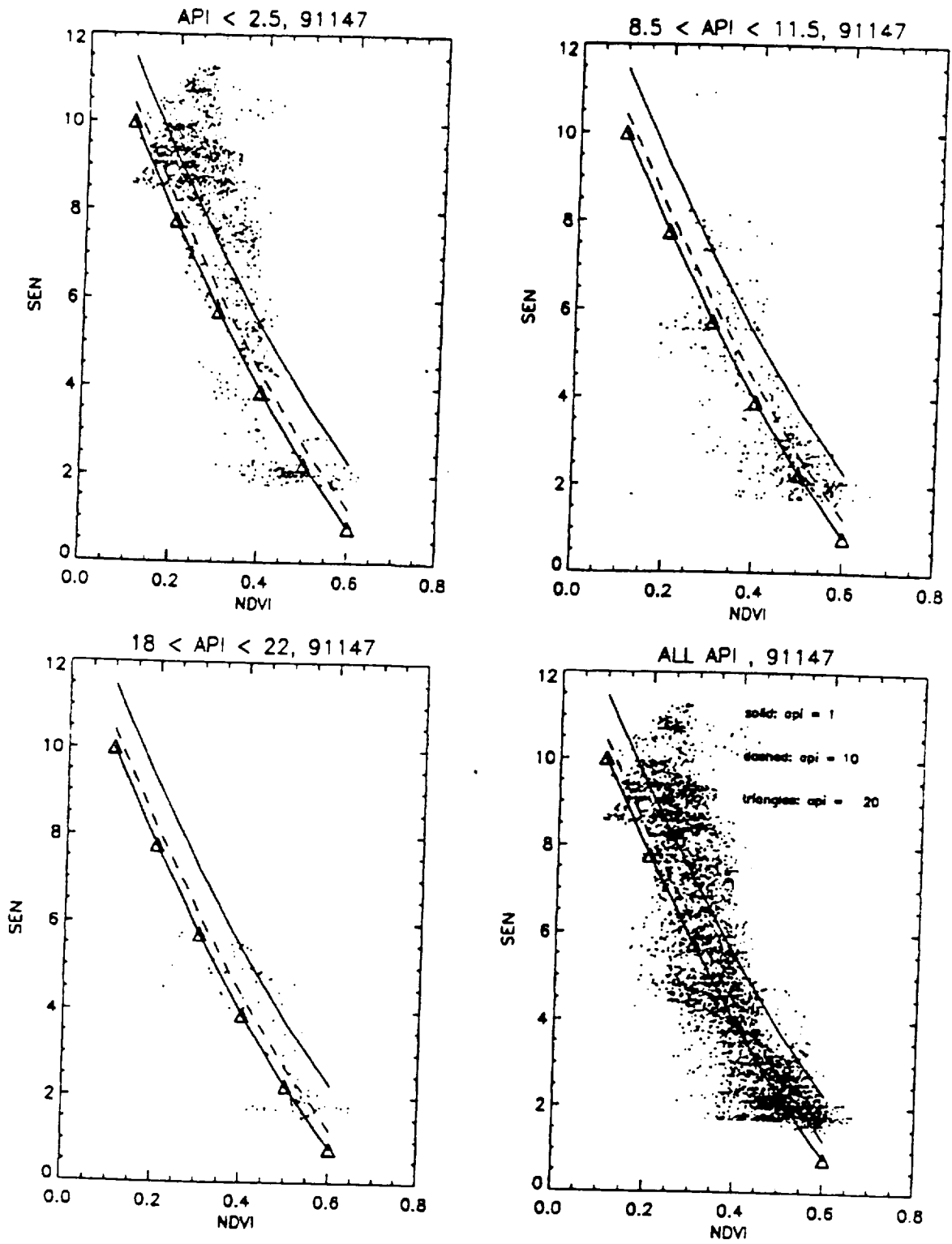


Fig. 8a

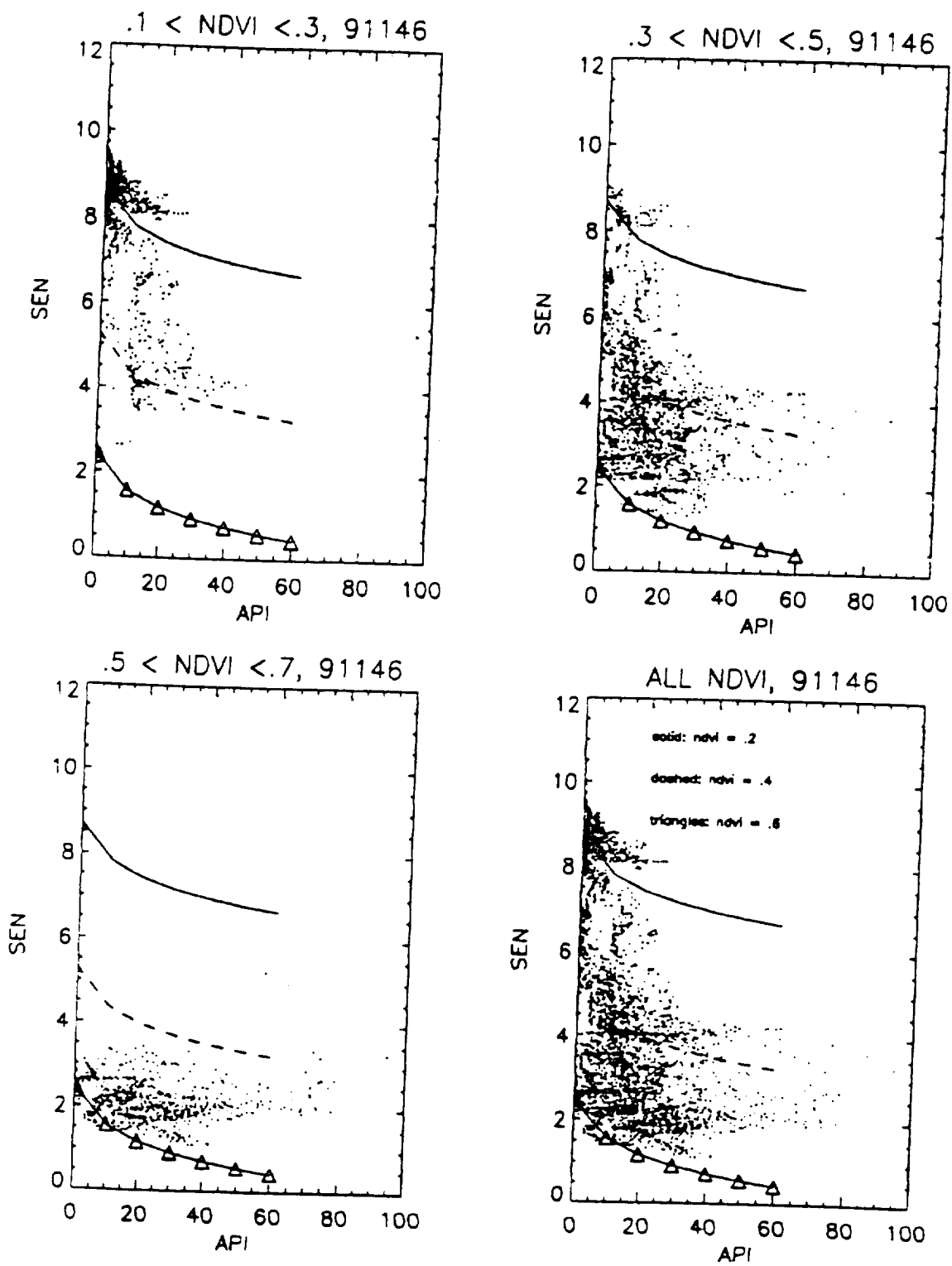


Fig. 8b

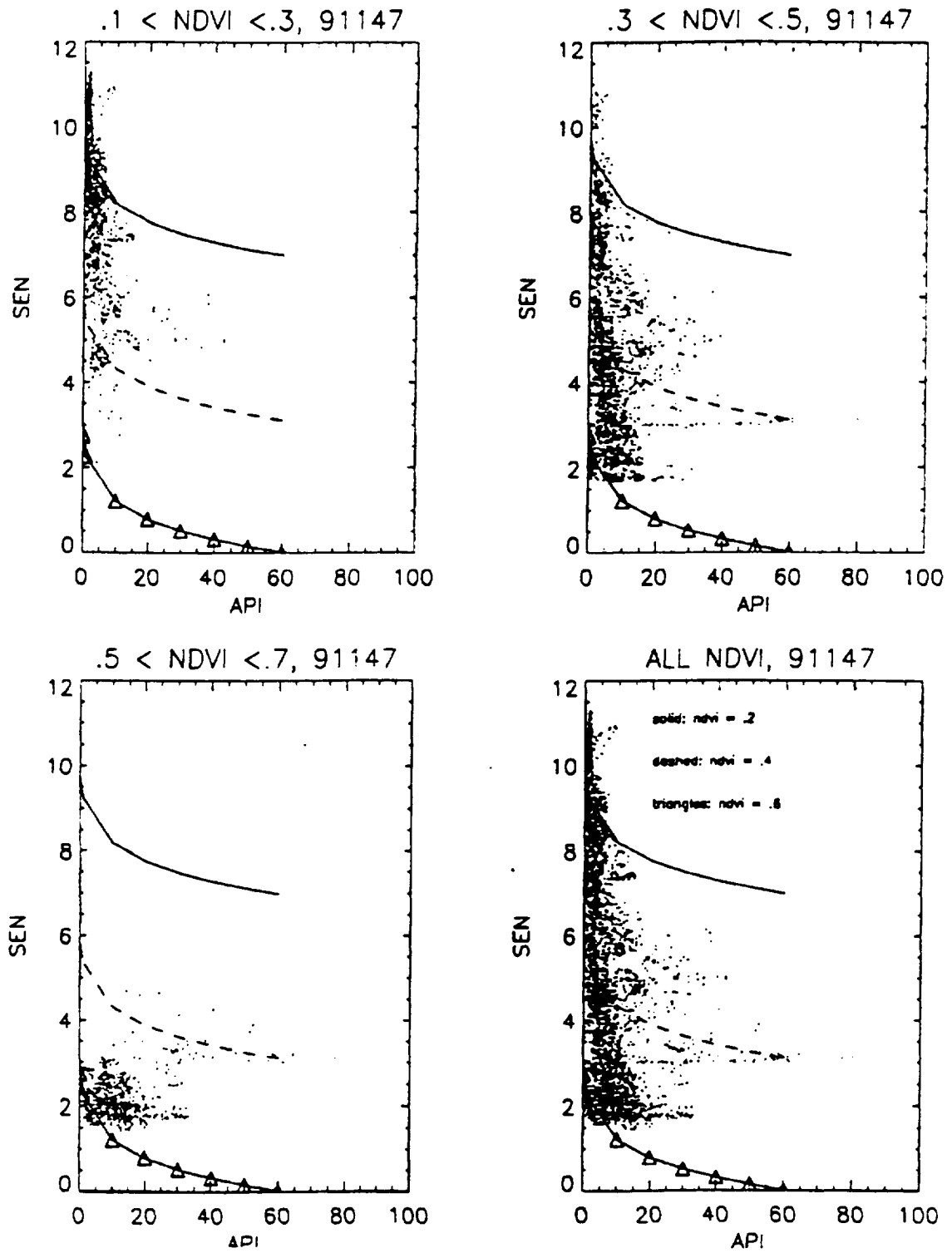


Fig. 9a

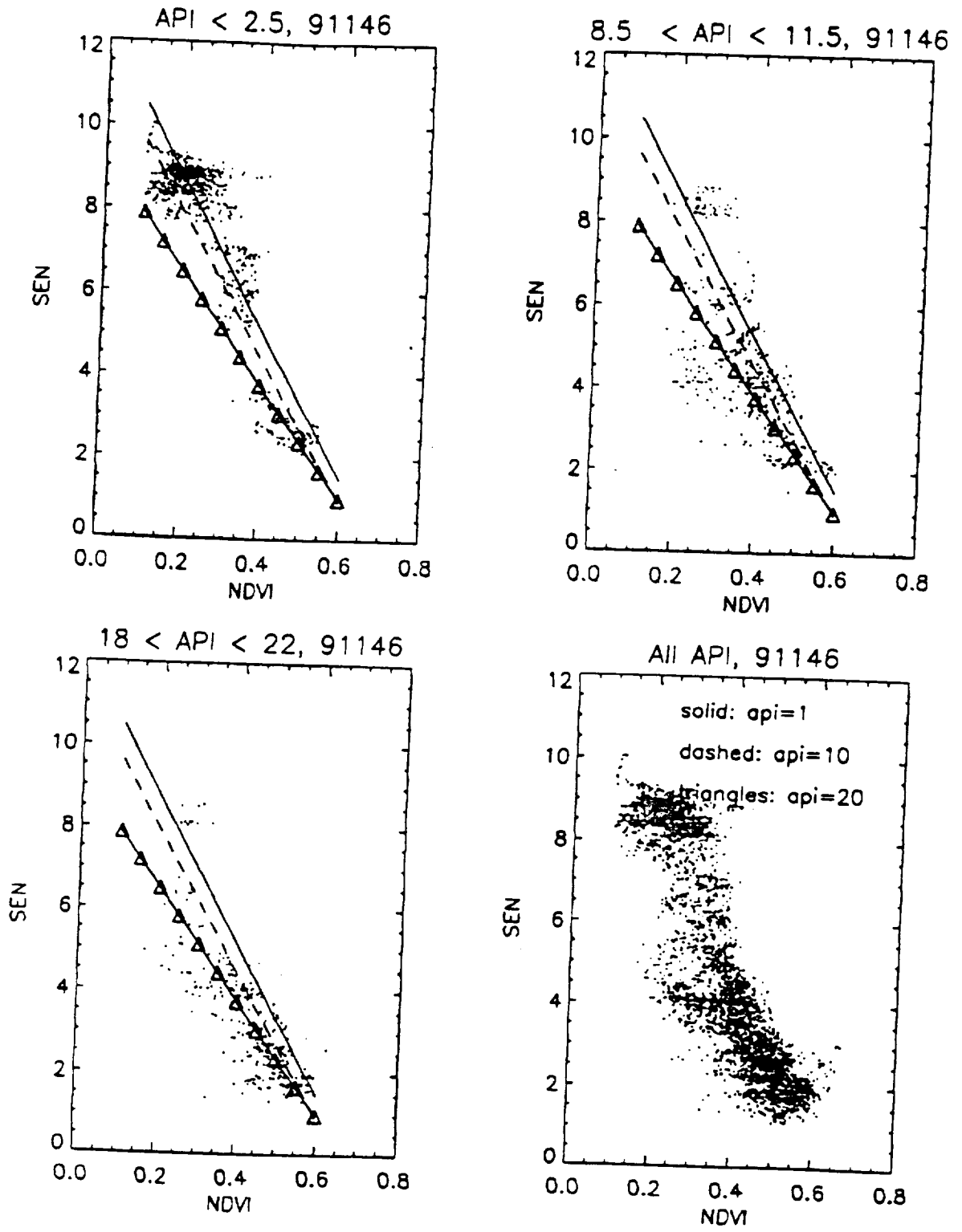


Fig. 9b

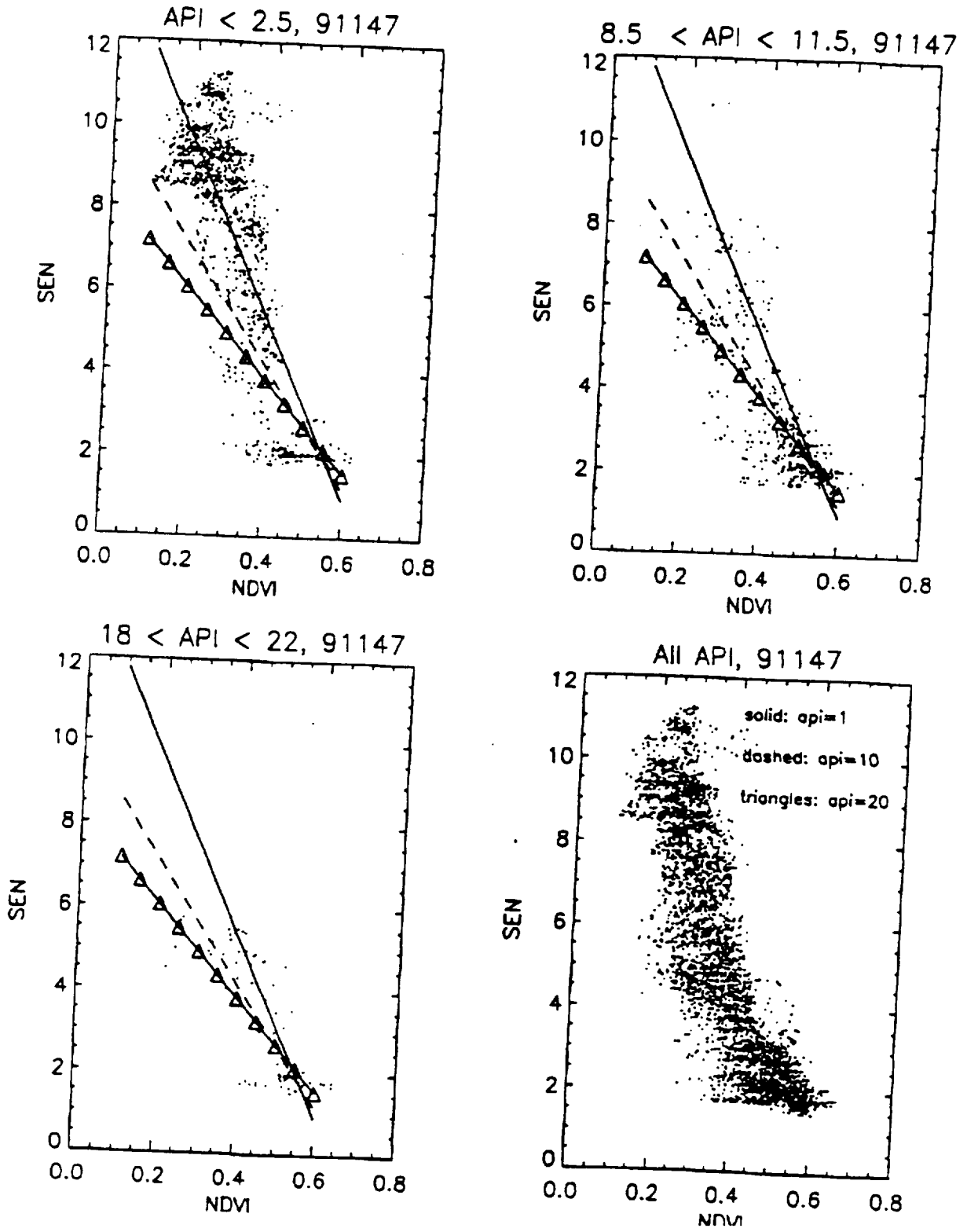


Fig. 10a

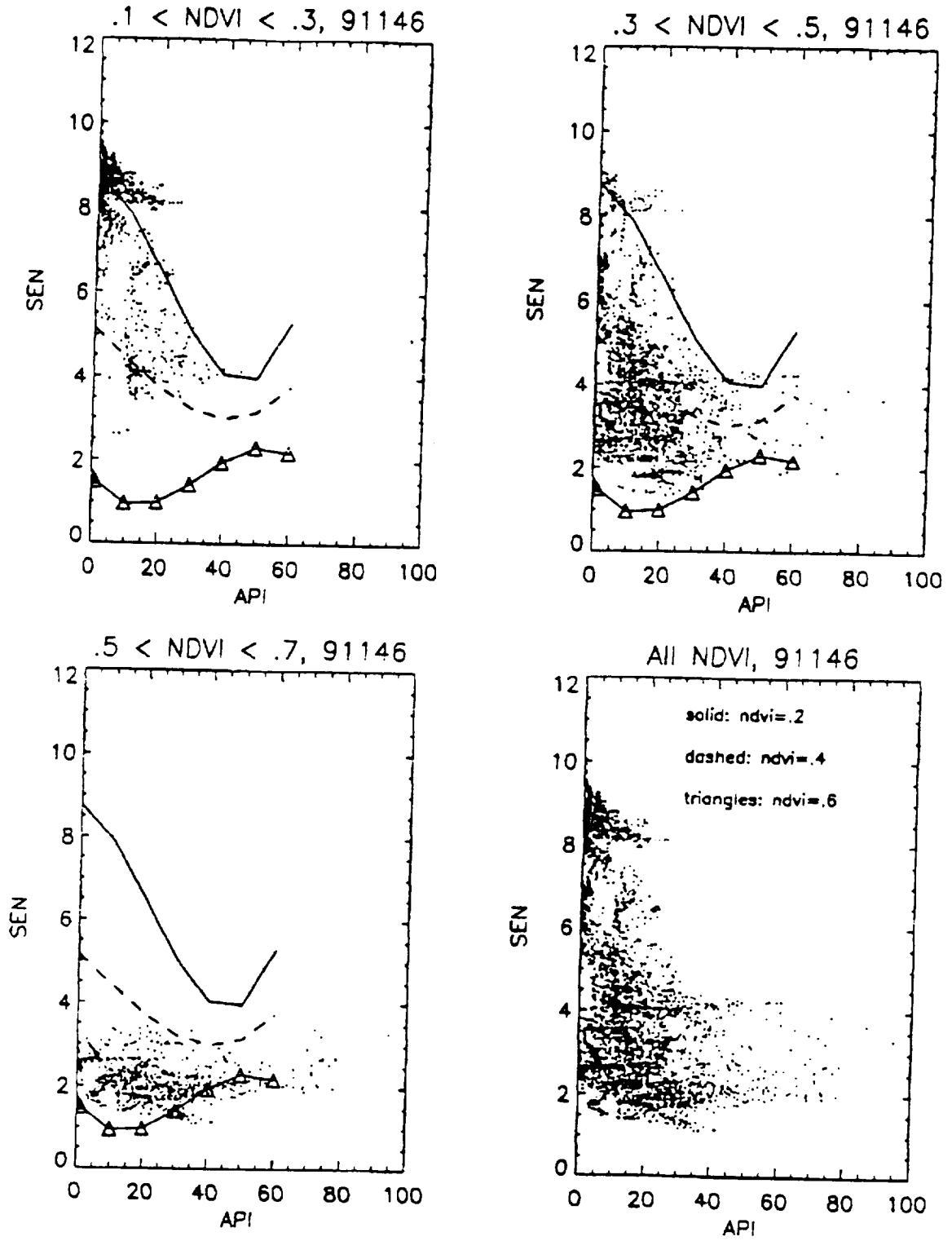


Fig. 10b

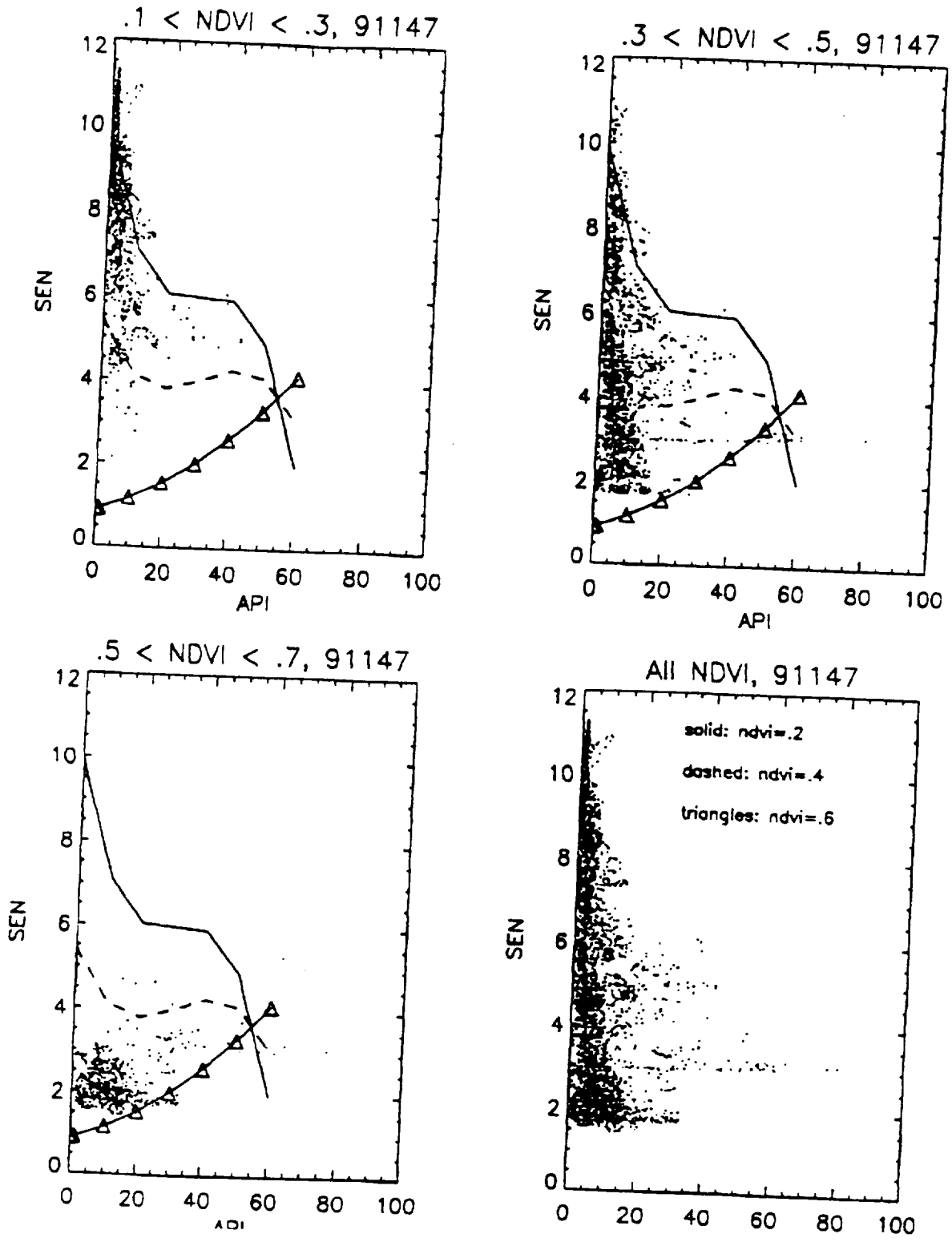


Fig. 11a

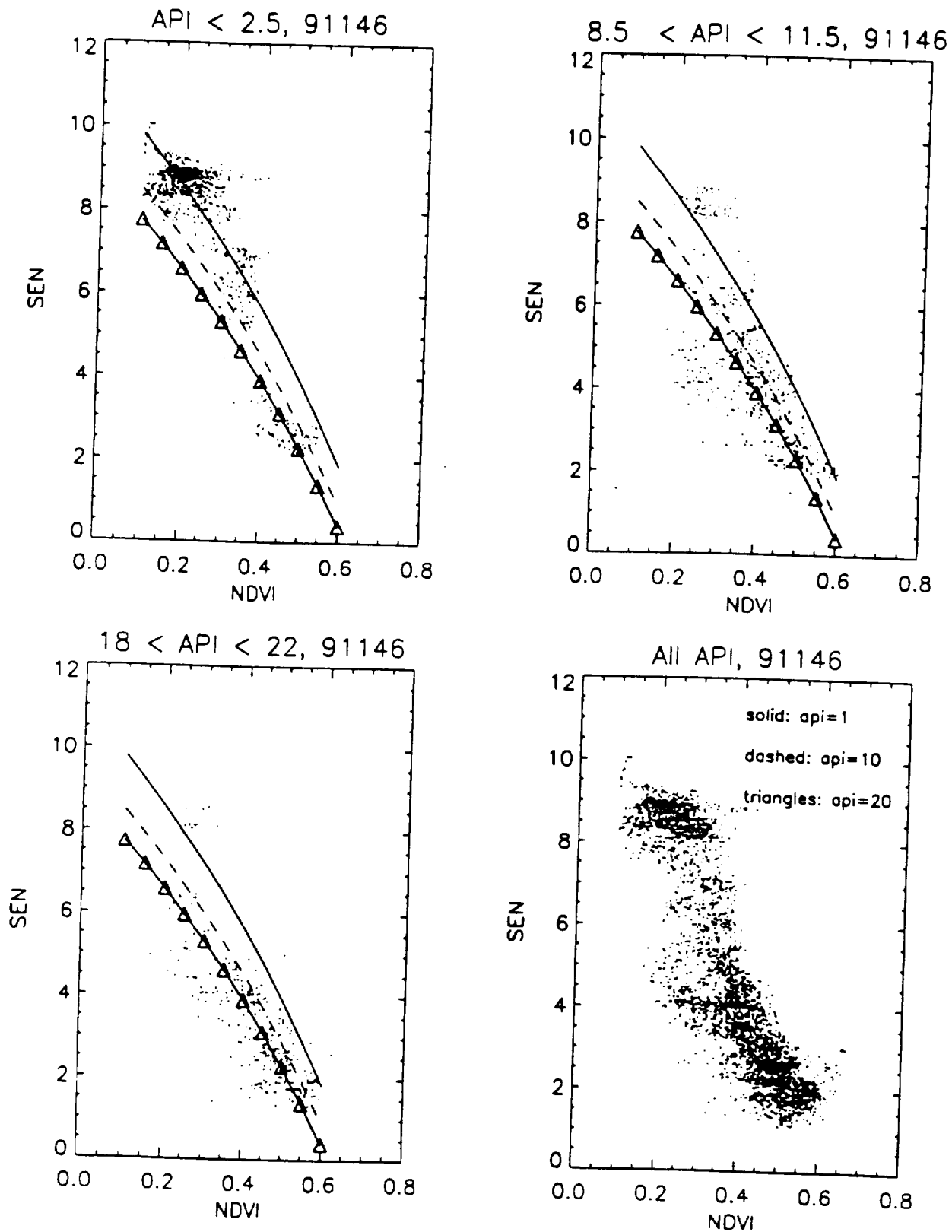


Fig. 11b

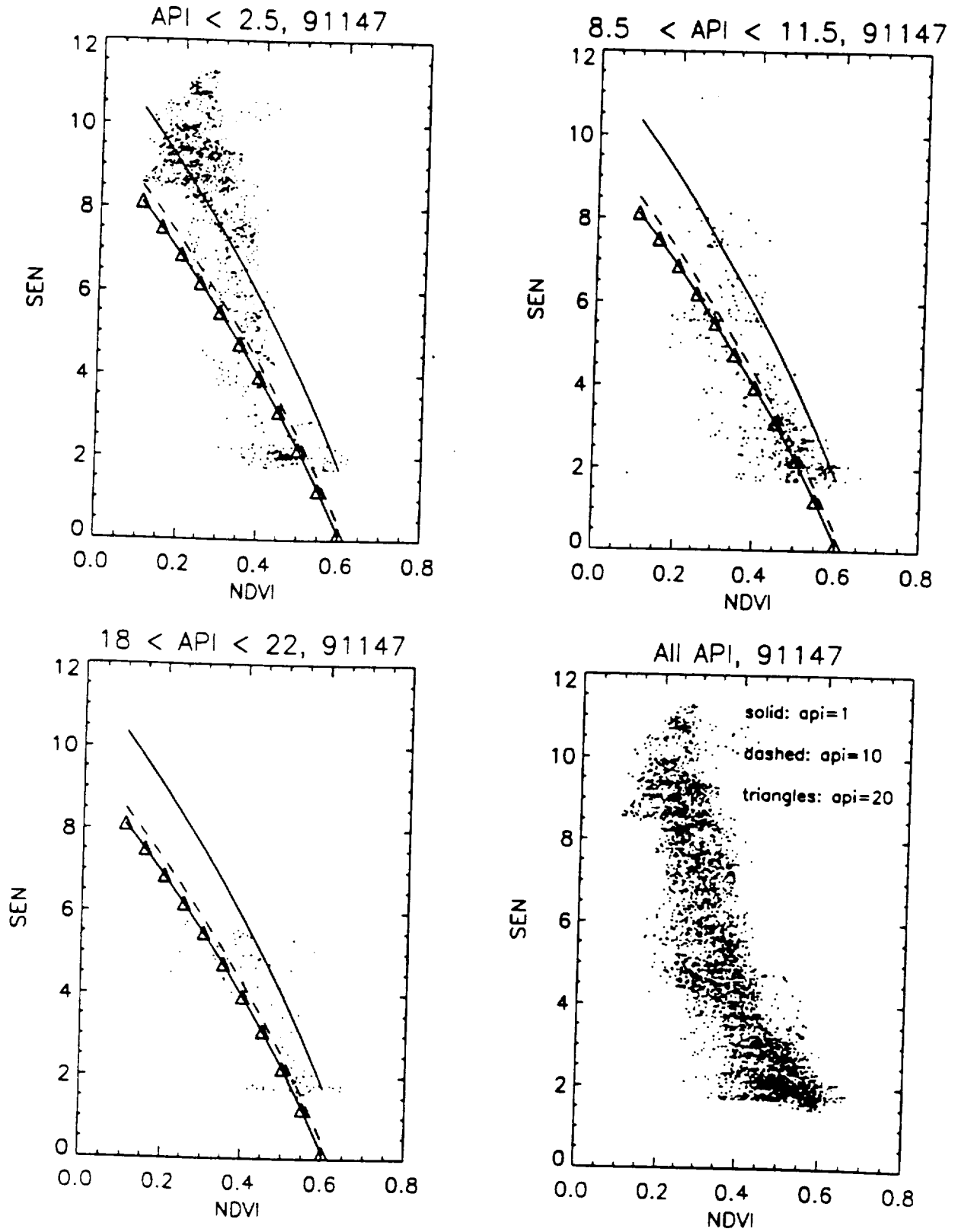


Fig. 12a

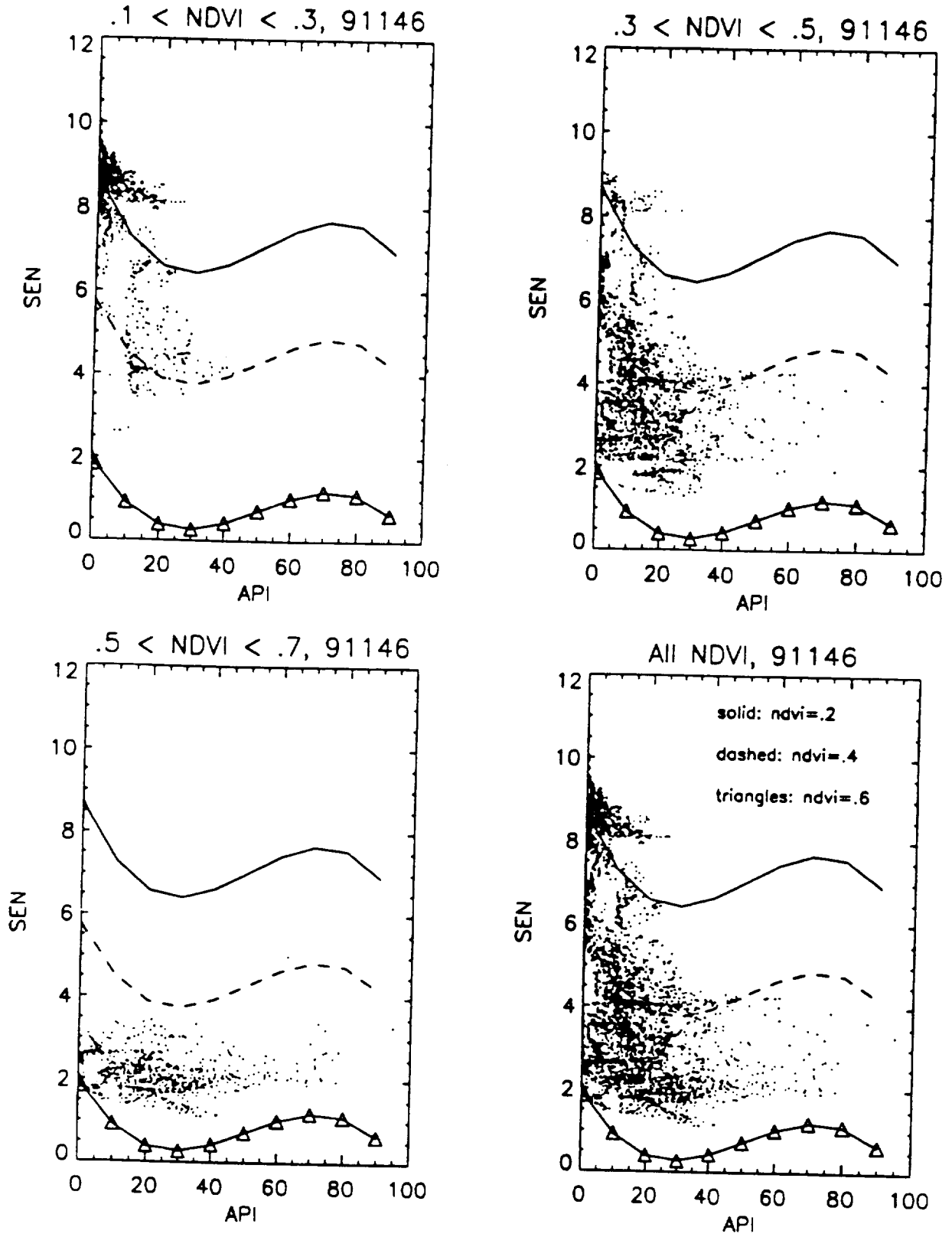


Fig. 12b

